Journal of Experimental Pharmacology

ISSN: 1179-1454 (Online) Journal homepage: www.tandfonline.com/journals/djep20

Multi-Target Anti-Steatotic Effects of Andrographolide in MAFLD: Insights from Network Pharmacology and in vitro Study

Hiba Adnan Aziz Abu Omaima, Abbas Hasan Burhan, Wiqar Adnan Azeez Aboomaima & Ali Mahmoudi

To cite this article: Hiba Adnan Aziz Abu Omaima, Abbas Hasan Burhan, Wiqar Adnan Azeez Aboomaima & Ali Mahmoudi (2026) Multi-Target Anti-Steatotic Effects of Andrographolide in MAFLD: Insights from Network Pharmacology and in vitro Study, Journal of Experimental Pharmacology, , 625161, DOI: 10.2147/JEP.S625161

To link to this article: https://doi.org/10.2147/JEP.S625161

Published online: 21 Aug 2026.

Journal of Experimental Pharmacology

Dovepress
Taylor & Francis Group

Open Access Full Text Article

ORIGINAL RESEARCH

Multi-Target Anti-Steatotic Effects of Andrographolide in MAFLD: Insights from Network Pharmacology and in vitro Study

Hiba Adnan Aziz Abu Omaima[1], Abbas Hasan Burhan[1], Wiqar Adnan Azeez Aboomaima[2], Ali Mahmoudi[3]

[1]College of Biotechnology, Al-Qadisiya University, Al-Diwaniya, Iraq; [2]College of Science, Al-Qadisiya University, Al-Diwaniya, Iraq; [3]Department of Basic Medical Sciences, Faculty of Medicine, Abadan University of Medical Sciences, Abadan, Iran

Correspondence: Ali Mahmoudi, Department of Basic Medical Sciences, Faculty of Medicine, Abadan University of Medical Sciences, Abadan, Iran, Email Alimahmoudi68@yahoo.com

Background: Metabolic Associated Fatty Liver Disease (MAFLD) is a prevalent metabolic disorder with no effective approved pharmacotherapy. Andrographolide, a bioactive diterpenoid from *Andrographis paniculata*, has anti-inflammatory and antioxidant properties, but its mechanisms in MAFLD remain unclear.

Methods: An integrated computational and experimental approach was applied. Network pharmacology was used to identify shared targets between andrographolide and MAFLD using public drug-target and disease databases. Protein-protein interaction analysis, pathway enrichment, and molecular docking with hub proteins were then performed. For experimental validation, hepatic steatosis was induced in HUH7 cells with oleic acid (1 mM, 24 h) and treated with andrographolide (14 μM). Lipid accumulation was measured by Oil Red O staining, and hub gene expression was analyzed by qRT-PCR.

Results: In silico analysis identified 253 shared targets, with TNF, IL6, AKT1, TP53, IL1B, JUN, VEGFA, STAT3, CASP3, and EGFR as major hubs. Enrichment analysis highlighted lipid metabolism, and inflammation signaling pathways. Molecular docking showed strong binding to AKT1 (–7.7 kcal/mol), EGFR (–7.5 kcal/mol), and STAT3 (–7.2 kcal/mol). In vitro, andrographolide reduced oleic acid-induced lipid accumulation by 38% ($p = 0.0032$). qRT-PCR revealed significant downregulation of AKT1 (73.5%, $p = 0.0159$), EGFR (72.0%, $p = 0.0137$), and STAT3 (53.6%, $p = 0.0220$) mRNA expression in andrographolide-treated steatotic hepatocytes. These transcript-level changes are correlative observations and do not confirm direct inhibition of AKT1, EGFR, or STAT3 protein activity, which requires phosphorylation-specific validation. The mRNA findings suggest a potential association between andrographolide treatment and modulation of these signaling pathways at the transcriptional level.

Conclusion: Andrographolide alleviates hepatic steatosis and is associated with transcriptional modulation of AKT1, EGFR, and STAT3 mRNA. However, protein-level validation is absent, and these findings should be considered hypothesis-generating rather than mechanistic proof of target inhibition. The results support further investigation of andrographolide as a potential multi-target therapeutic candidate for MAFLD.

Keywords: andrographolide, fatty liver disease, molecular docking, bioinformatics, gene expression, HUH7 cells

Introduction

Metabolic dysfunction-associated fatty liver disease (MAFLD), formerly known as nonalcoholic fatty liver disease (NAFLD), impacts roughly 25% of the global population and encompasses a progressive continuum from hepatic steatosis to metabolic dysfunction-associated steatohepatitis (MASH), fibrosis, cirrhosis, and hepatocellular carcinoma.[1–5] This condition is closely associated with obesity, insulin resistance, and type 2 diabetes, serving as an independent risk factor for cardiovascular diseases and extrahepatic malignancies due to systemic proinflammatory and profibrotic environments.[2,6,7] The complexity of the disease is further exacerbated by dysregulated metabolic pathways, such as bile acid metabolism and nuclear receptor signaling, which play significant roles in disease progression and the severity of fibrosis.[8,9] Despite its increasing prevalence

https://doi.org/10.2147/JEP.S625161
Received: 16 May 2026
Accepted: 12 August 2026
Published: 21 August 2026

Graphical Abstract

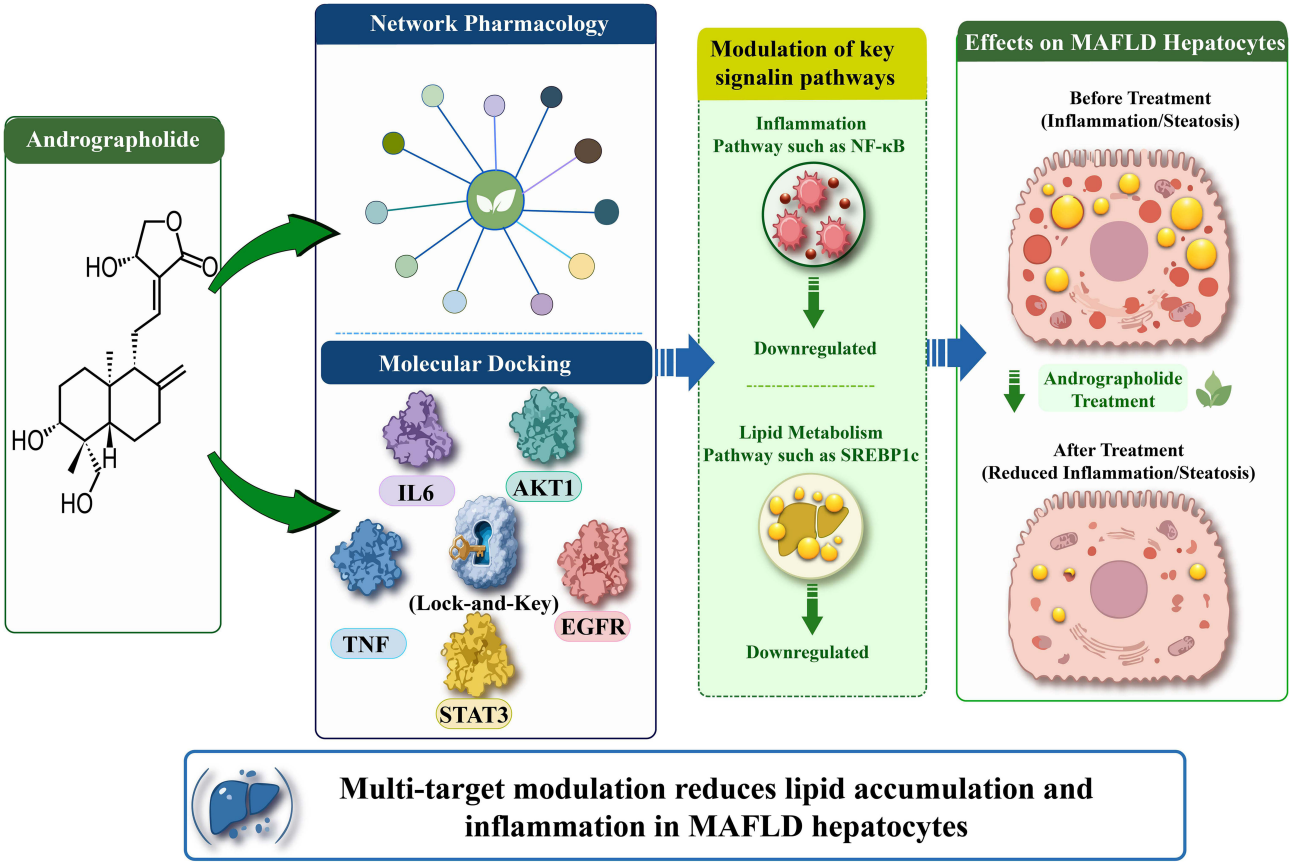

and multisystemic effects, there are currently no approved pharmacological treatments for MAFLD/MASH, highlighting an urgent clinical demand for innovative therapeutic approaches.[1,10]

Andrographolide, the primary bioactive diterpenoid lactone extracted from Andrographis paniculata, has attracted considerable interest due to its extensive pharmacological properties, particularly its strong anti-inflammatory and antioxidant effects.[11–14] Indeed, andrographolide is considered the principal active component of *A. paniculata*, demonstrating protective and therapeutic benefits in various liver disease models.[14] Mechanistically, andrographolide inhibits Nuclear factor kappa B (NF-κB) signaling, reduces the expression of pro-inflammatory cytokines (Interleukin (IL)-1β, IL-6, Tumor necrosis factor (TNF)-α), and activates the Nrf2-mediated antioxidant response, which are essential for mitigating chronic inflammation and oxidative stress associated with metabolic diseases.[11,14–18] Recent findings also suggest that andrographolide influences glucose and lipid metabolism, thereby expanding its therapeutic potential beyond conventional anti-inflammatory roles.[11]

Experimental models of MAFLD have confirmed the effectiveness of andrographolide. In mice subjected to a high-fat diet (HFD), the administration of andrographolide resulted in a reduction of obesity, an improvement in glucose tolerance, and a decrease in hepatic steatosis through the downregulation of FATP2-mediated fatty acid uptake.[19]

Simultaneously, it inhibits adipogenic differentiation by interfering with the CCAAT/enhancer-binding protein beta (C/EBPβ) / Peroxisome proliferator-activated receptor gamma (PPARγ) signaling pathways.[20,21] Additionally, its derivative, 14-deoxy-11,12-didehydroandrographolide, has been shown to alleviate steatohepatitis by enhancing antioxidant activities.[22] In MASH models, andrographolide has been found to diminish hepatic inflammation, hepatocyte ballooning, and fibrosis by inhibiting the NLRP3 inflammasome and modulating TLR4/NF-κB and TGF-β/Smad signaling pathways.[23]

Moreover, synergistic anti-fibrotic effects have been noted when used in conjunction with pirfenidone, which acts by blocking the activation of hepatic stellate cells.[24] Comprehensive hepatoprotective effects have also been reported across various liver injury models, including cirrhosis, alcoholic liver disease, and drug-induced fibrosis.[17,25–27] Despite the challenges posed by poor bioavailability that impede clinical application, innovative nanocarrier delivery systems hold potential for improving its therapeutic efficacy.[10,28]

Due to the fact that natural products such as andrographolide frequently interact with multiple molecular targets, contemporary research is increasingly utilizing computational "in silico" techniques to forecast their mechanisms of action. Network pharmacology, molecular docking, and associated bioinformatics tools amalgamate extensive databases and systems biology to delineate drug-target-pathway networks.[29–32] Recent integrative research that merges computational predictions with experimental validation has effectively elucidated the mechanisms of andrographolide across a range of diseases. For instance, network pharmacology has been employed to clarify the effects of various traditional Chinese medicinal compounds on complex diseases, including MAFLD. In a recent investigation, researchers integrated network analysis with molecular docking to unravel andrographolide's role in hepatocellular carcinoma.[33] By forecasting andrographolide's potential protein targets and subsequently validating significant interactions through docking simulations, they pinpointed pertinent signaling pathways impacted by the compound.[33] Furthermore, Zhang et al (2025) illustrated that andrographolide mitigates acute liver injury through the NOD-like receptor protein 3 (NLRP3)/Caspase-1/ Gasdermin D (GSDMD)-mediated pyroptosis pathway, utilizing network pharmacology and molecular docking techniques.[34] Yin et al (2025) applied integrative network pharmacology alongside in vivo and in vitro experiments to uncover andrographolide's influence on the Signal transducer and activator of transcription 3 (STAT3)/ Phosphoinositide 3-kinase (PI3K)/Akt pathways in diabetic nephropathy.[35] More recently, Zhang et al (2026) discovered prostaglandin E synthase 3 (Ptges3) as a covalent target of andrographolide, indicating the disruption of the Ptges3-Hsp90-NF-κB axis in pulmonary fibrosis.[36] These investigations underscore the efficacy of combined computational and experimental methodologies in clarifying multi-target mechanisms and validating innovative therapeutic pathways.

Although prior research has demonstrated the effectiveness of andrographolide in MAFLD through distinct pathways (eg, Fatty acid transport protein (FATP)2, Transforming Growth Factor (TGF)-β, NLRP3), there is a notable absence of a comprehensive systems-level analysis that identifies the key hub genes and core signaling networks concurrently targeted by andrographolide in this context. Our research addresses this significant gap by: (i) utilizing network pharmacology to develop an integrated drug-target-disease interaction network, which prioritizes hub genes and essential biological pathways pertinent to the pathogenesis of MAFLD, including potential targets related to cell cycle regulation (CDT1, CDC6),[37] inflammatory modulation (galectin-3),[38] and metabolic regulation (pregnane X receptor (PXR));[9] (ii) offering novel pathway-level evidence through extensive functional enrichment analyses that uncover interconnected signaling networks beyond isolated pathway mechanisms; and (iii) We are confirming the changes in expression of prioritized hub genes in a well-established MAFLD cell culture model through real-time PCR. These transcript-level observations are correlative and do not establish direct functional inhibition of the encoded proteins. Although these mRNA changes indicate a link between andrographolide treatment and the modulation of these signaling pathways, we recognize that they might also represent secondary responses to decreased cellular steatosis. This method adds another layer of validation that supports existing in vivo studies, but more functional experiments are necessary to establish direct causal relationships. This dual computational-experimental framework not only consolidates current mechanistic insights but also identifies new candidate targets and pathway interactions that have not been previously reported in MAFLD, providing a prioritized roadmap for future mechanistic exploration and therapeutic development.

Methods

Data Acquisition and Target Identification for Andrographolide

The potential protein targets of Andrographolide (CID: 5318517) were systematically gathered from seven prominent pharmacological and cheminformatics databases to guarantee thorough coverage. The databases that were queried include: SwissTargetPrediction (probability > 0.097), SEA (Similarity Ensemble Approach, Affinity Threshold (nM) > 5), PubChem BioActivity, PPB2 (Protein-Protein-Binding) database, BindingDB, IUPHAR/BPS Guide to Pharmacology,

and PharmMapper (Fit score > 2.0). Gene symbols corresponding to the predicted targets were extracted from the output of each database. Duplicate entries were eliminated, resulting in a unique and non-redundant list of targets associated with Andrographolide.

In silico Toxicity Prediction of Andrographolide

A computational assessment of the toxicity of the compound Andrographolide was conducted using two complementary in silico platforms, ProTox 3.0 and ADMETlab 3.0, to create a detailed profile. Initially, the structure of Andrographolide was input into the ProTox 3.0 server by its common name. The compound underwent analysis through an ensemble of 61 machine-learning models.[39] Molecular similarity was evaluated against databases of known toxic substances, and fragment propensities were computed to pinpoint structural motifs linked to toxicity. Predictions regarding binding to specific toxicity targets were made using a collection of protein-ligand-based pharmacophore models. Consequently, predictions for acute oral toxicity (LD50), organ toxicity, and various toxicological endpoints were derived. Simultaneously, a distinct evaluation was performed utilizing the ADMETlab 3.0 platform. The compound was analyzed through a Directed Message Passing Neural Network (DMPNN) framework to assess a broad range of properties. Predictions were produced for 21 physicochemical parameters, 19 medicinal chemistry properties, 34 ADME endpoints, and 36 toxicity endpoints. Furthermore, the structure was screened against a set of 751 toxicophore rules to detect any undesirable substructures. Ultimately, the findings from both analyses were integrated and interpreted. Consensus alerts were recognized, and a unified in silico toxicity profile for Andrographolide was assembled to evaluate its potential liabilities.

MAFLD-Related Target Gene Collection

Genes linked to MAFLD were sourced from three specific disease databases: DisGeNET (version 2020) (GDA score > 0.01), Pharos (meanRankScore > 1), and GeneCards (relevance score > 0.145). The search utilized the terms "Non-Alcoholic Fatty Liver Disease" or "MAFLD." To maintain data integrity, targets from GeneCards were filtered according to a relevance score. The final compilation of MAFLD-related genes was achieved by merging the findings from all three databases and eliminating duplicates.

Identification of Shared Targets

The shared targets between Andrographolide and MAFLD, which signify potential direct therapeutic intervention points, were determined by calculating the intersection of the two gene lists derived from sections 2.2.1 and 2.2.2. A Venn diagram was created to illustrate the overlap.

Protein-Protein Interaction (PPI) Network and Hub Gene Analysis

The list of shared targets was uploaded to the STRING database (version 11.5) to develop a PPI network. The analysis focused on Homo sapiens with a minimum interaction score threshold of 0.400 (medium confidence). Isolated nodes were excluded from the network. The resulting network was downloaded and subjected to further analysis using the igraph package in R. Network topology metrics, such as degree, betweenness centrality, and closeness centrality, were computed for each node. Hub genes were identified as the top 10 nodes exhibiting the highest degree centrality. This threshold was selected based on established practice in network pharmacology studies, where the top 10 nodes by degree centrality are commonly recognized as the most influential hubs.[40,41] Furthermore, the Louvain algorithm was employed for community detection within the network to uncover densely connected clusters of proteins, which may indicate functional modules.

Functional and Pathway Enrichment Analysis

To elucidate the biological functions, pathways, and processes influenced by the common targets, a thorough enrichment analysis was conducted. The shared gene symbols were transformed into Entrez IDs utilizing the org.Hs.eg.db database.

The subsequent enrichment analyses were executed employing the clusterProfiler package: Kyoto Encyclopedia of Genes and Genomes (KEGG) Pathway Analysis aimed to identify significantly enriched signaling pathways (organism: "hsa"). Reactome Pathway Analysis was performed to reveal enriched pathways within the Reactome knowledgebase. Gene

Ontology (GO) Enrichment Analysis was carried out to categorize genes into three distinct categories: Biological Process (BP), Molecular Function (MF), and Cellular Component (CC). For all analyses, a p-value threshold of < 0.05 and a q-value threshold of < 0.1 were established as criteria for statistical significance. The outcomes were illustrated through dot plots and enrichment maps.

All data processing and statistical analyses were conducted utilizing R software (version 4.5.0). Visual representations, which included UpSet plots (for set intersections), Venn diagrams, PPI networks, and bar charts for hub genes, were created using packages such as ggplot2, ggraph, ggvenn, and UpSetR.

Molecular Docking Analysis

To explore the potential direct binding interactions between Andrographolide and the significant MAFLD-related targets identified through the network pharmacology analysis, in silico molecular docking simulations were conducted using AutoDock Vina integrated within PyRx software (version 1.0).

Ligand and Protein Preparation

The two-dimensional (2D) configuration of Andrographolide (CID: 5318517) was sourced from the PubChem database. Subsequently, this configuration underwent energy minimization and was converted into its three-dimensional (3D) representation using PyRx software. The three-dimensional representations of the key hub proteins, which include TNF, IL6, AKT1, TP53, IL1B, JUN, VEGFA, STAT3, CASP3, and EGFR, were retrieved from the AlphaFold database to ensure the generation of high-quality predictive models. All protein structures were prepared for docking through the DockPrep module, which entailed the removal of water molecules and heteroatoms, the incorporation of polar hydrogen atoms, and the assignment of Kollman charges.

Docking Protocol

Molecular docking was executed using PyRx software (version 1.0), which employs the AutoDock Vina algorithm for predicting binding poses. Due to the absence of co-crystallized ligands with clearly defined binding pockets in the AlphaFold models, a blind docking approach was utilized, enabling andrographolide to investigate the entire surface of the protein.[42] A large grid box was established for each target protein, with dimensions adequate to encompass the entire protein structure. The center of the grid was strategically placed at the geometric center of each protein to facilitate comprehensive sampling. To promote extensive exploration of conformational space and improve the reliability of the results, the exhaustiveness parameter was elevated to 80, a figure significantly greater than the default value of 8, which markedly enhances the thoroughness of sampling and the reproducibility of docking outcomes (Trott and Olson, 2010). For each protein target, nine distinct binding modes (num_modes = 9) were produced. For each protein target, multiple docking runs were conducted, and the pose with the most favorable (lowest) binding energy (ΔG, kcal/mol) was chosen for further analysis.

To validate the docking protocol, the consistency of predicted binding modes across multiple docking runs was assessed. For each target protein, nine binding modes were generated, and the RMSD (root-mean-square deviation) between different predicted poses was calculated. The selection of the lowest-energy pose (rmsd/ub = 0) for each target followed standard practice in structure-based virtual screening.

To validate the reliability and accuracy of our docking protocol, a re-docking experiment was performed using the crystal structure of AKT1 (PDB ID: 4GV1), which contains a co-crystallized ligand (AZD5363, residue code 0XZ). The ligand was extracted from the crystal structure, and the protein was prepared following the same protocol as for the AlphaFold models (removal of water molecules, addition of polar hydrogens, and assignment of Kollman charges). The ligand was re-docked into the binding site using AutoDock Vina with identical parameters. The re-docked pose was then compared to the crystallographic pose using the bio3d package (version 2.4–5) in R (version 4.5.0). Hydrogen atoms were removed from both ligands, and the structures were superimposed using the fit.xyz function to achieve optimal alignment. The RMSD between the re-docked and crystallographic ligand poses was calculated using the rmsd function, with an RMSD value below 2.0 Å considered acceptable, confirming the protocol's ability to reproduce known binding poses.[43]

Interaction Analysis

The docking poses generated for each Andrographolide-protein complex were examined and visualized utilizing Discovery Studio Visualizer (version 4.5). This analysis aimed to clarify the distinct molecular interactions, especially hydrogen bonds, hydrophobic contacts, and ionic interactions, that play a role in the stability of the complexes. The binding energy associated with each complex served as the main criterion for assessing the binding affinity, where more negative values signify a stronger binding.

Cell Culture and Treatment Conditions

The human hepatoma cell line HUH7 was sourced from the Pasteur Institute of Iran (Tehran, Iran) and was maintained in RPMI-1640 medium (Gibco, USA) enriched with 10% fetal bovine serum (FBS; Gibco) and 1% penicillin-streptomycin solution. The cells were cultured at 37°C in a humidified environment with 5% CO_2 and were passaged using trypsin-EDTA once they reached approximately 80% confluency. Cells from passages 4–14 were utilized for all experimental procedures.

Induction of Steatosis with Oleic Acid

In the course of the experimental procedures, cells were plated in 24-well plates at a density of 5×10^4 cells per well and allowed to adhere for a duration of 24 hours. Hepatic steatosis was induced by treating the cells with 1 mM oleic acid (OA; Sigma-Aldrich, USA)[31] complexed with bovine serum albumin (BSA) at a molar ratio of 6:1 for 24 hours. The OA-BSA complex was freshly prepared in serum-free RPMI medium by warming the mixture to 37°C for 10 minutes with gentle agitation, followed by sterile filtration through a 0.22 μm membrane. Control cells were treated with BSA alone at equivalent concentrations.

Drug Treatments

For the therapeutic interventions, cells were concurrently treated with 1 mM OA and 14 μM andrographolide[1] (Sigma-Aldrich, USA) for a period of 24 hours. Andrographolide was initially dissolved in dimethyl sulfoxide (DMSO) and subsequently diluted in the culture medium to ensure a final DMSO concentration of less than 0.1%.

Evaluation of Lipid Accumulation

Intracellular lipid accumulation was assessed through Oil Red O (ORO) staining, following previously established protocols with some modifications. After the treatments, cells were subjected to two washes with phosphate-buffered saline (PBS) and subsequently fixed in 4% paraformaldehyde for 15 minutes at room temperature. Post-fixation, the cells were rinsed with distilled water and treated with 60% isopropanol for 5 minutes to improve the specificity of lipid staining. The cells were then stained with a 0.5% Oil Red O solution, which was prepared by diluting a stock solution in isopropanol with distilled water at a 3:2 ratio, for 30 minutes at room temperature. Any excess dye was eliminated by washing with distilled water until the background appeared clear. For semi-quantitative analysis, the stained lipids were eluted by incubating the cells in 100% isopropanol for 10 minutes. The absorbance of the eluted dye was recorded at 500 nm using a microplate reader (BioTek Synergy H1, USA). A total of three independent experiments were conducted, each comprising three biological replicates for each treatment group.

RNA Isolation and qRT-PCR Analysis

Total RNA was extracted from both treated and control cells utilizing the RNAX-PLUS reagent, with its concentration and purity (A260/A280 ratio of 1.9–2.1) confirmed using a NanoDrop 2000 spectrophotometer. For each sample, 1 μg of total RNA underwent reverse transcription into cDNA employing the Easy cDNA Synthesis Kit. Quantitative real-time PCR (qRT-PCR) was conducted on a LightCycler® 96 system in 20 μL reactions that included SYBR Green Master Mix, 10 ng of cDNA, and 0.5 μM of gene-specific primers. The gene-specific primers for AKT1 (Forward: 5′-TACGAGATGATGTGCGGTCG-3′, Reverse: 5′-CAGTGTAGTCTGGGAGGTGC-3′), EGFR (Forward: 5′-ACCAGTCCGTTCCCAAAAGG-3′, Reverse: 5′-GCTGGTAGTCAGGGTTGTCC-3′), and STAT3 (Forward: 5′-TTCCTTTCCCCGTTTTGCCT-3′, Reverse: 5′-ATGGTATTGCTGCAGGTCGT-3′) were designed using Primer3 (NCBI) and their specificity was validated through Primer-BLAST. The housekeeping gene GAPDH (Forward: 5′-CTCTGACTTCAACAGCGAC-3′, Reverse: 5′-

CGTTGTCATACCAGGAAATGAG-3′) acted as the endogenous control for normalizing target gene expression using the comparative ΔΔCT method. GAPDH was chosen because it is widely recognized as a reliable reference gene in hepatocyte models of steatosis.[31,44] This gene was used for normalization. To confirm the validity of normalization in our experimental setup, we evaluated the Cq values of GAPDH across different treatment groups. The thermal cycling profile included an initial denaturation step (95°C, 10 min), followed by 50 cycles of denaturation (95°C, 10 sec) and a combined annealing/extension phase (60°C, 45 sec). A melting curve analysis was performed to confirm the specificity of the amplification. All reactions were executed in triplicate. The relative expression levels were determined using the comparative ΔΔCT method, with the OA-treated group serving as the calibrator.

Statics Analysis

All statistical analyses were conducted utilizing R statistical software version 4.5.0. Data derived from both Oil Red O absorbance measurements and ΔCT values are expressed as mean ± standard error of the mean (SEM) from three independent experiments. To validate the normalization for qRT-PCR, we evaluated the stability of GAPDH expression across different treatment groups by comparing the raw Cq values using one-way ANOVA followed by Tukey's post-hoc test. The normality of data distribution was evaluated using Shapiro–Wilk tests, while the homogeneity of variances was verified through Levene's tests. For the planned comparisons, two-tailed independent Student's t-tests were utilized to assess: (1) the differences between OA-treated and Control cells to validate steatosis induction, and (2) the differences between OA+Andrographolide and OA-treated cells to evaluate therapeutic efficacy. Effect sizes were computed as Cohen's d with 95% confidence intervals to measure the magnitude of the observed differences. Statistical significance was established at $p < 0.05$. No multiple testing correction was applied as these comparisons were pre-planned and hypothesis-driven.

Results

In silico ADMET Profiling of Andrographolide

The absorption, distribution, metabolism, excretion, and toxicity (ADMET) profile of andrographolide was predicted using in silico methods to assess its drug-likeness and potential pharmacokinetic issues. The primary findings are illustrated in Figure 1 and elaborated upon below.

Physicochemical Properties and Drug-Likeness

Andrographolide (molecular weight: 350.21 g/mol) demonstrates advantageous physicochemical characteristics that suggest good cellular permeability. The compound shows moderate lipophilicity (calculated LogP = 2.48) and a significant topological polar surface area (TPSA = 86.99 $Å^2$). It complies with Lipinski's rule of five (0 violations), indicating a high likelihood of oral bioavailability. Nevertheless, its predicted aqueous solubility is low (LogS = −4.26), which may restrict its absorption. The structure is relatively inflexible (number of rotatable bonds = 3) and contains a high proportion of sp^3 carbons (Fsp3 = 0.75), traits commonly linked to successful clinical candidates.

Pharmacokinetic Properties (ADME)

The anticipated ADME profile indicates several important features. Andrographolide is expected to exhibit low permeability in Caco-2 and MDCK cell models (Log apparent permeability < −5.3), implying potential difficulties in intestinal absorption. It is forecasted to have low plasma protein binding (Fu = 33.8%) and a moderate volume of distribution (VDss = −0.30 L/kg), suggesting a propensity to distribute into tissues rather than remain in systemic circulation. Importantly, the compound is predicted to be a substrate for the efflux transporter P-glycoprotein (Pgp-sub probability = 0.009), which may further restrict its oral absorption and brain penetration (BBB permeability probability = 0.28). The compound is not anticipated to inhibit major cytochrome P450 enzymes, with the highest likelihood of inhibition noted for CYP2C8 (0.89) and CYP2C9 (0.062), indicating a low risk for drug-drug interactions through this pathway.

Toxicity Profile

The in-silico toxicity evaluation produced varied outcomes. A notable concern is the elevated predicted probability for carcinogenicity (0.98) and genotoxicity (0.99), which necessitates further experimental scrutiny. The compound demonstrated a low probability of inhibiting the hERG channel (0.22), indicating a minimal risk for QT interval prolongation

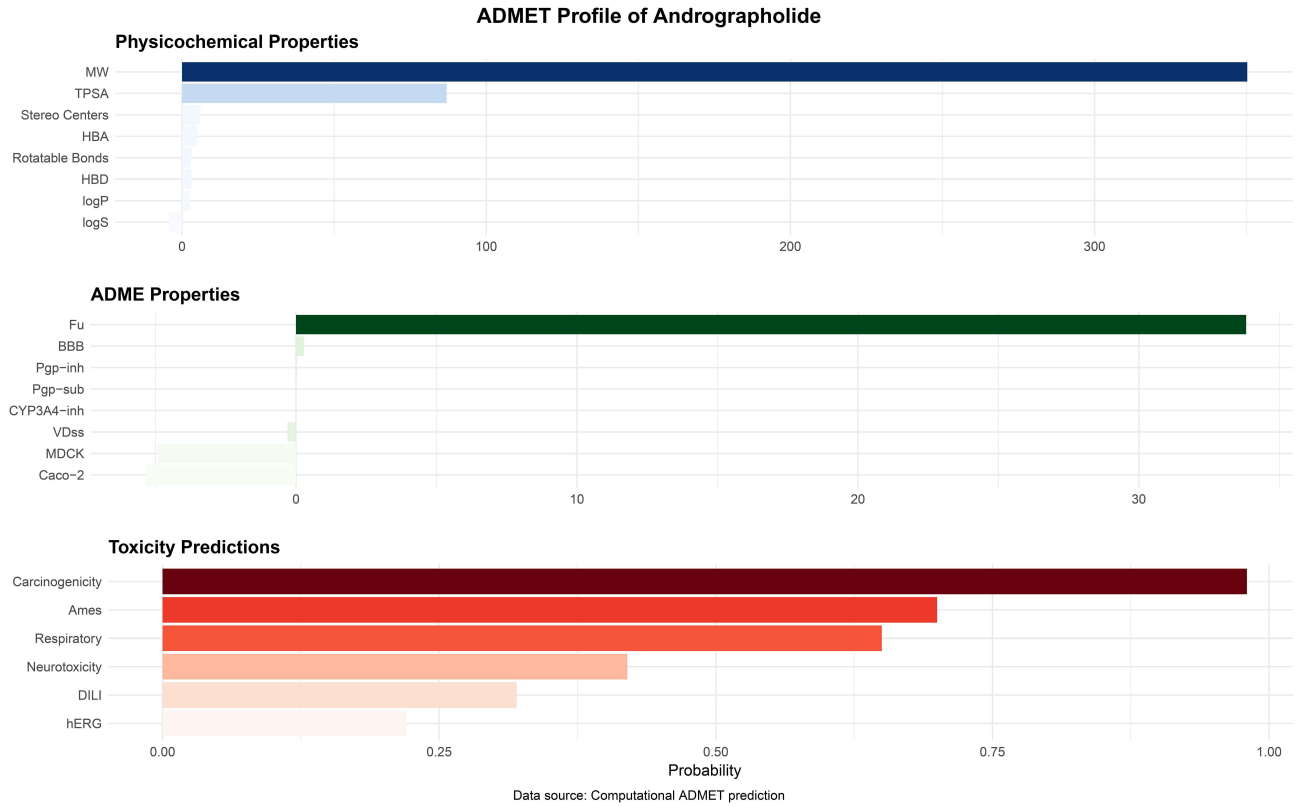

Figure 1 Computational assessment of essential physicochemical, pharmacokinetic (ADME), and toxicity characteristics profile of Andrographolide.

and related cardiotoxic effects. It was predicted to yield a negative result in the Ames test (probability = 0.70, where values > 0.5 typically suggest a negative outcome), which aligns with its established status as a natural product but contrasts with the genotoxicity prediction, underscoring the necessity for confirmatory assays. The likelihood of drug-induced liver injury (DILI) was predicted to be low (probability = 0.32).

To evaluate the possible harmful effects of Andrographolide, an in silico toxicity analysis was conducted utilizing the ProTox-3.0 web platform (Figure 2).

The model estimated the median lethal dose (LD50) for Andrographolide to be 1890 mg/kg. According to the Globally Harmonized System (GHS) of classification, this figure categorizes Andrographolide within Toxicity Class 4, defined as "Harmful if swallowed" (LD50> range: 500–5000 mg/kg). The prediction was achieved with an accuracy of 69.26% and an average similarity of 70.04% to established compounds in the database.

The findings from various toxicity models are compiled in Table 1. Andrographolide was predicted to be inactive in several significant organ toxicity endpoints, particularly hepatotoxicity (Probability: 0.93), neurotoxicity (0.94), and nephrotoxicity (0.51). Additionally, it was forecasted to be non-carcinogenic, non-mutagenic, and non-cytotoxic. Nevertheless, the compound was predicted to exhibit activity in a subset of endpoints including Respiratory Toxicity (Active, Probability: 0.68), Cardiotoxicity (Active, Probability: 0.55), Immunotoxicity (Active, Probability: 0.82), Clinical Toxicity (Active, 0.67), and Nutritional Toxicity (Active, 0.84) (Table 1).

Nuclear Receptor Signaling, Stress Response, and Molecular Initiating Events

Andrographolide was forecasted to exhibit inactivity across all 25 targets within the Tox21 nuclear receptor signaling pathways (for instance, ER, AR, PPAR-γ) and stress response mechanisms (including p53). Furthermore, it was also anticipated to be inactive concerning all molecular initiating events, such as interactions with thyroid hormone receptors, ion channels (RYR, GABA, NMDA), and various enzymes.

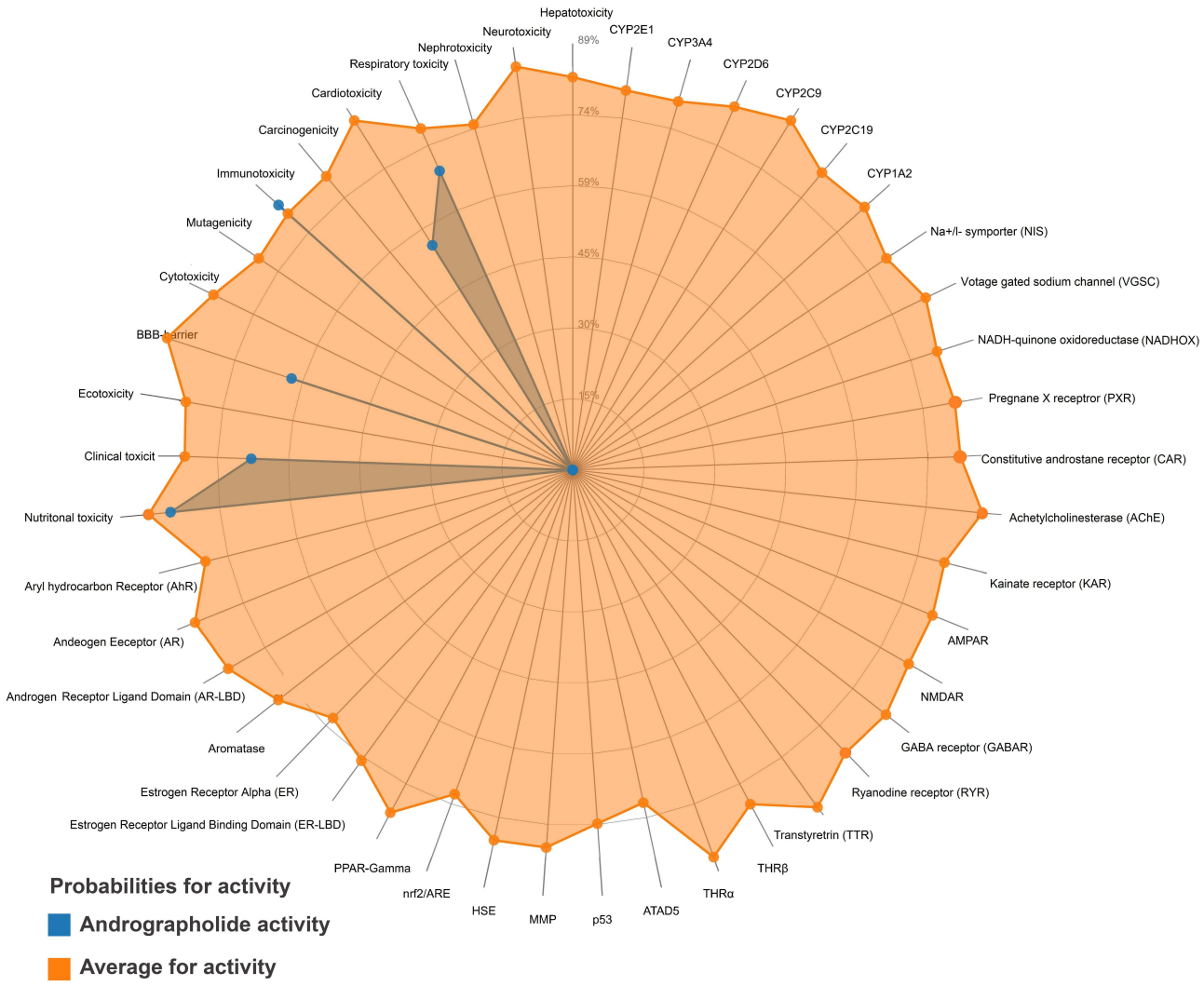

Figure 2 Radar chart depicting the anticipated toxicity profile of Andrographolide across significant endpoints, as produced by ProTox 3.0. The chart illustrates the probability of activity for each toxicity model, emphasizing a favorable prediction of inactivity regarding hepatotoxicity and cytochrome P450 inhibition.

Drug Metabolism and Kinetics

Importantly, Andrographolide was predicted to be inactive as an inhibitor of all principal cytochrome P450 enzymes (CYP1A2, 2C9, 2C19, 2D6, 2E1, and 3A4), with probabilities ranging from 0.77 to 0.99. This indicates a minimal likelihood of pharmacokinetic drug-drug interactions resulting from CYP enzyme inhibition.

Table 1 Overview of Key ProTox-3.0 Predictions for Andrographolide

Toxicity Model	Prediction	Probability	Interpretation
Acute Oral Toxicity (LD50)	Class 4	–	1890 mg/kg (Harmful)
Hepatotoxicity	Inactive	0.93	Low risk of liver injury
Neurotoxicity	Inactive	0.94	Low risk of neurotoxicity
Carcinogenicity	Inactive	0.83	Non-carcinogenic
Mutagenicity	Inactive	0.71	Non-mutagenic
Immunotoxicity	Active	0.82	Potential immunotoxic effect
Cardiotoxicity	Active	0.55	Potential cardiotoxic effect
CYP Inhibition (All)	Inactive	>0.77	Low risk of cytochrome P450 inhibition

https://doi.org/10.2147/JEP.S625161

Comprehensive Target Profiling Reveals Shared Molecular Targets Between Andrographolide and MAFLD

Through integrative analysis of multiple pharmacological and disease databases, we identified 788 potential protein targets of andrographolide and 2,060 MAFLD-associated targets across ten specialized databases. The target distribution varied significantly across databases, with GeneCards containing the largest number of MAFLD targets (1,299) and the BindingDB database containing the fewest andrographolide targets.[4]

Notably, we discovered 253 shared targets between andrographolide and MAFLD, representing 32.11% of all andrographolide targets (Figure 3). This substantial overlap suggests a strong potential molecular basis for andrographolide's therapeutic effects on MAFLD. The details regarding the overlapping proteins are included in Supplementary Table S1.

Analysis of the Protein-Protein Interaction Network Reveals Essential Hub Genes and Functional Modules

The constructed PPI network from shared targets has unveiled a sophisticated interaction framework comprising 250 nodes and 4,372 edges (refer to Figure 4a). An examination of the network's topology has pinpointed ten pivotal hub genes based on their degree centrality: TNF (degree=330), IL6 (318), AKT1 (312), TP53 (302), IL1B (274), JUN (270), VEGFA (262), STAT3 (258), CASP3 (258), and EGFR (248) (see Figure 4b and Table 2). These hub genes serve as central regulators within the network and may play a significant role in the therapeutic effects of andrographolide on MAFLD.

The community detection analysis conducted using the Louvain algorithm has identified four distinct functional modules within the PPI network (illustrated in Figure 4a): Community 1 (79 nodes): This community is enriched in signaling transduction and cell cycle regulation, featuring key components such as MAPK1/3/14, STAT3, TP53, EGFR, and JUN. Community 2 (52 nodes): This module is primarily engaged in metabolic processes, encompassing xenobiotic metabolism (CYP450 family), antioxidant defense (SOD1/2, CAT), and glutathione metabolism (GSTM1, GSTP1). Community 3 (83 nodes): This community focuses on inflammatory responses and immune regulation, highlighting TNF, IL6, IL1B, MMPs, and various chemokines. Community 4 (36 nodes): This module is dedicated to lipid metabolism and nuclear receptor signaling, including members of the PPAR family, FABPs, and NR1H receptors.

Pathway Enrichment Analysis Uncovers Mechanisms of Action

To shed light on how andrographolide works therapeutically in MAFLD and to confirm the biological significance of our target selection, we conducted KEGG and Reactome pathway enrichment analyses on both the overlapping targets (andrographolide ∩ MAFLD) and the complete MAFLD gene set.

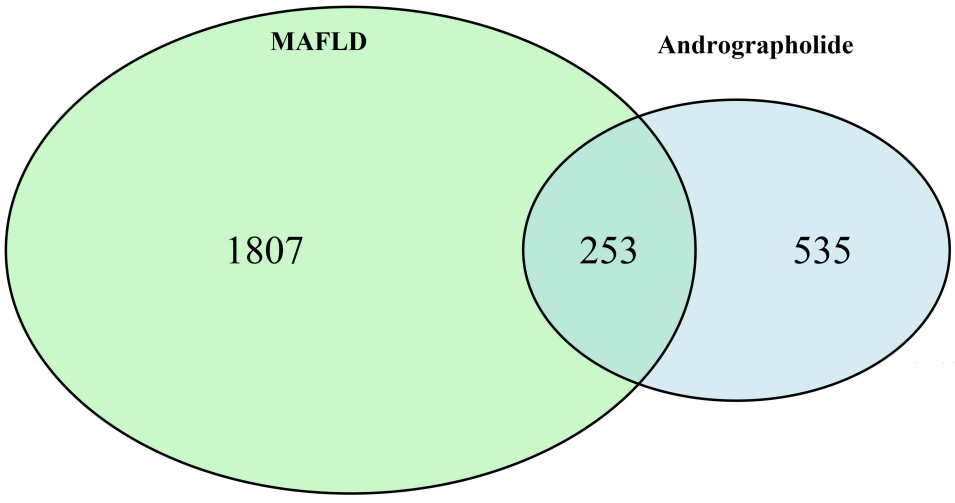

Figure 3 Intersection between MAFLD and Andrographolide.

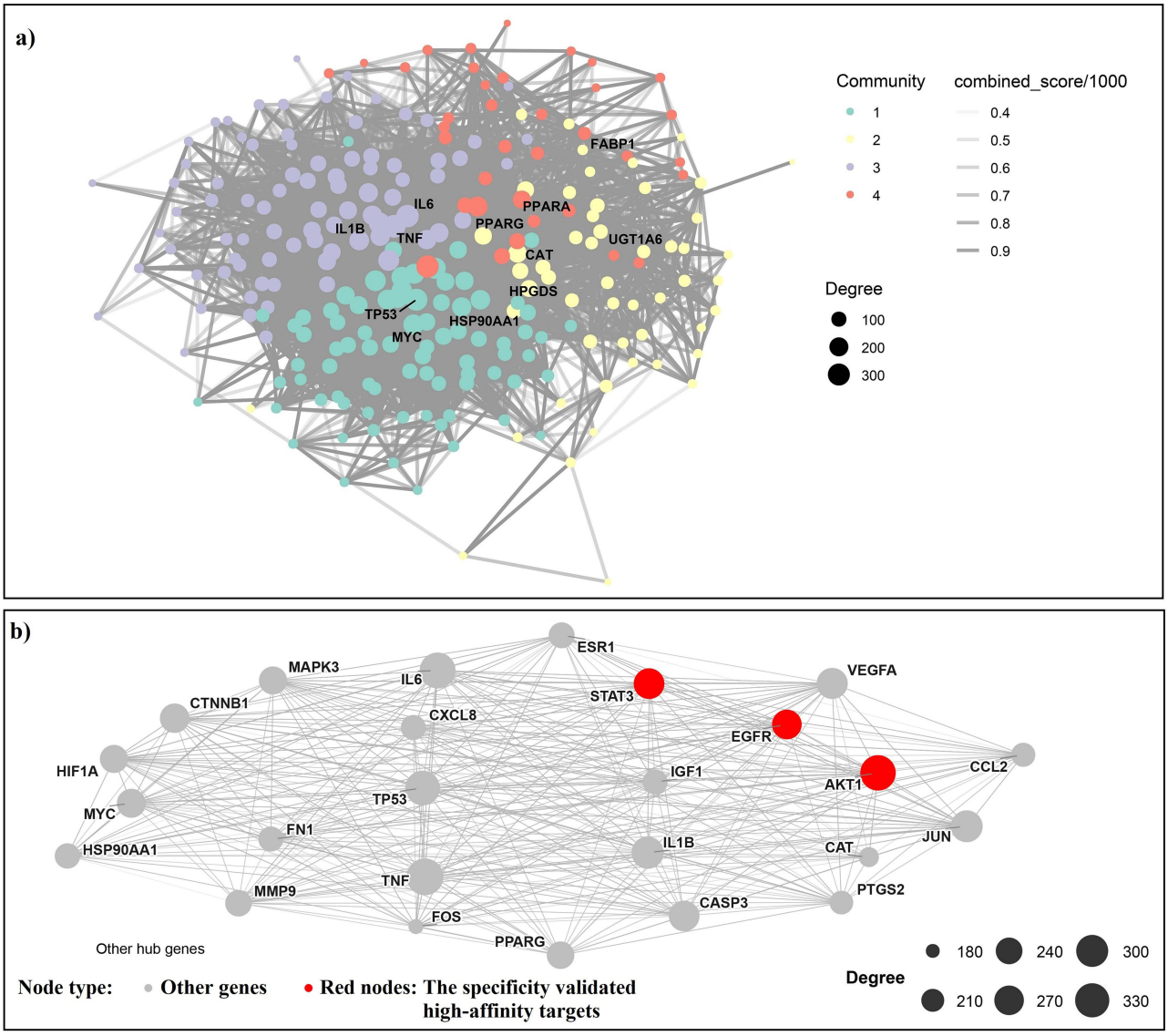

Figure 4 (**a**) Protein-Protein Interaction (PPI) Network and Functional Modules of Shared Targets. Nodes are color-coded according to four distinct functional modules identified by the Louvain algorithm, each represented in different colors. Number of node: 250, Number of edges: 10646, Number of communities: 4. (**b**) Top 20 Hub gene PPI network with centrality metrics. Node size and color represent Degree and validated high-affinity targets, respectively (scale shown). The three docking-validated targets (AKT1, STAT3, EGFR) are highlighted as red color.

Pathway Enrichment Analysis of Shared Targets

KEGG pathway analysis revealed significant enrichment in various pathways pertinent to MAFLD (Figure 5a). The pathway with the highest level of enrichment was "Lipid and atherosclerosis" (hsa05417, $p=7.93\times10^{-39}$), followed by "AGE-RAGE signaling pathway in diabetic complications" (hsa04933, $p=4.27\times10^{-32}$), and "Hepatitis B" (hsa05161, $p=1.87\times10^{-28}$). Notably, "Non-alcoholic fatty liver disease" (hsa04932) exhibited significant enrichment ($p=2.30\times10^{-19}$), with 32 common targets associated with this pathway.

Reactome pathway analysis further validated these results (Figure 5b), highlighting "Signaling by Interleukins" (R-HSA-449147, $p=3.24\times10^{-31}$) and "Interleukin-4 and Interleukin-13 signaling" (R-HSA-6785807, $p=1.12\times10^{-30}$) as the most significantly enriched pathways. Additionally, the pathways "Programmed Cell Death" (R-HSA-5357801, $p=1.06\times10^{-14}$) and "Cellular response to chemical stress" (R-HSA-9711123, $p=1.06\times10^{-14}$) were also significantly enriched.

https://doi.org/10.2147/JEP.S625161

Table 2 Centrality Index of the PPI Network for the Intersection of MAFLD and Andrographolide Target Genes

Gene	Degree	Betweenness	Closeness
TNF	**330**	1.88E+03	2.99E-03
IL6	**318**	1.59E+03	2.93E-03
AKT1	**312**	1.26E+03	2.91E-03
TP53	302	1.18E+03	2.87E-03
IL1-B	274	8.83E+02	2.75E-03
JUN	270	6.47E+02	2.74E-03
VEGFA	262	5.18E+02	2.71E-03
STAT3	258	5.23E+02	2.69E-03
CASP3	258	5.05E+02	2.70E-03
EGFR	248	7.66E+02	2.65E-03

Notes: Bold values in the Degree column indicate the top three genes with the highest degree centrality, representing the most connected nodes within the protein-protein interaction (PPI) network.
Abbreviations: PPI, Protein-Protein Interaction; MAFLD, Metabolic dysfunction–associated fatty liver disease.

Comparative Pathway Enrichment Analysis with Full MAFLD Gene Set

To ensure that our shared targets were biologically relevant and that important MAFLD signals were not overlooked, we carried out an independent pathway enrichment analysis on the entire MAFLD gene set (n = 1,845 genes). The KEGG pathway that stood out the most in the full MAFLD gene set was "Lipid and atherosclerosis" (hsa05417), which included 113 enriched genes (GeneRatio = 113/1380, Fold Enrichment = 3.58, $p = 1.07 \times 10^{-39}$), aligning with the top pathway we found in our shared targets. Likewise, "Insulin resistance" (hsa04931) showed significant enrichment with 67 genes (Fold Enrichment = 4.20, $p = 1.51 \times 10^{-29}$), and "Non-alcoholic fatty liver disease" (hsa04932) had 76 genes (Fold Enrichment = 3.31, $p = 3.65 \times 10^{-24}$). The "TNF signaling pathway" (hsa04668) was also notably enriched with 69 genes (Fold Enrichment = 3.97, $p = 3.44 \times 10^{-28}$), highlighting the crucial role of inflammatory signaling in MAFLD (Figure 5c). Further analysis of the full MAFLD gene set using Reactome pathways reinforced these results, with "Signaling by Interleukins" (R-HSA-449147) emerging as the most significantly enriched pathway, comprising 162 genes (Fold Enrichment = 2.51, $p = 9.76 \times 10^{-32}$). Additionally, "Interleukin-4 and Interleukin-13 signaling" (R-HSA-6785807) was also notably enriched with 62 genes (Fold Enrichment = 4.09, $p = 4.76 \times 10^{-26}$). Pathways related to lipid metabolism, such as "Plasma lipoprotein assembly, remodeling, and clearance" (R-HSA-174824, 46 genes, Fold Enrichment = 4.37, $p = 2.56 \times 10^{-21}$) and "FOXO-mediated transcription" (R-HSA-9614085, 36 genes, Fold Enrichment = 3.95, $p = 5.38 \times 10^{-15}$) also showed significant enrichment (Figure 5d). This really highlights the important roles that lipid dysregulation and insulin signaling play in MAFLD.

Gene Ontology Analysis Clarifies Biological Functions

Gene Ontology analysis indicated significant enrichment in biological processes, molecular functions, and cellular components associated with the pathogenesis and treatment of MAFLD. In terms of biological processes, the most significantly enriched terms were "response to lipopolysaccharide" (GO:0032496, $p=4.05\times10^{-40}$), "response to molecule of bacterial origin" (GO:0002237, $p=6.06\times10^{-39}$), and "cellular response to biotic stimulus" (GO:0071216, $p=1.21\times10^{-31}$) (Figure 6a). These results imply that andrographolide may influence immune responses and inflammatory processes in MAFLD. Molecular function analysis demonstrated enrichment in "DNA-binding transcription factor binding" (GO:0140297, $p=3.46\times10^{-13}$), "phosphatase binding" (GO:0019902, $p=3.46\times10^{-13}$), and "nuclear receptor activity" (GO:0004879, $p=3.46\times10^{-13}$), suggesting that andrographolide has the potential to modulate transcriptional activity and signaling pathways (Figure 6b).

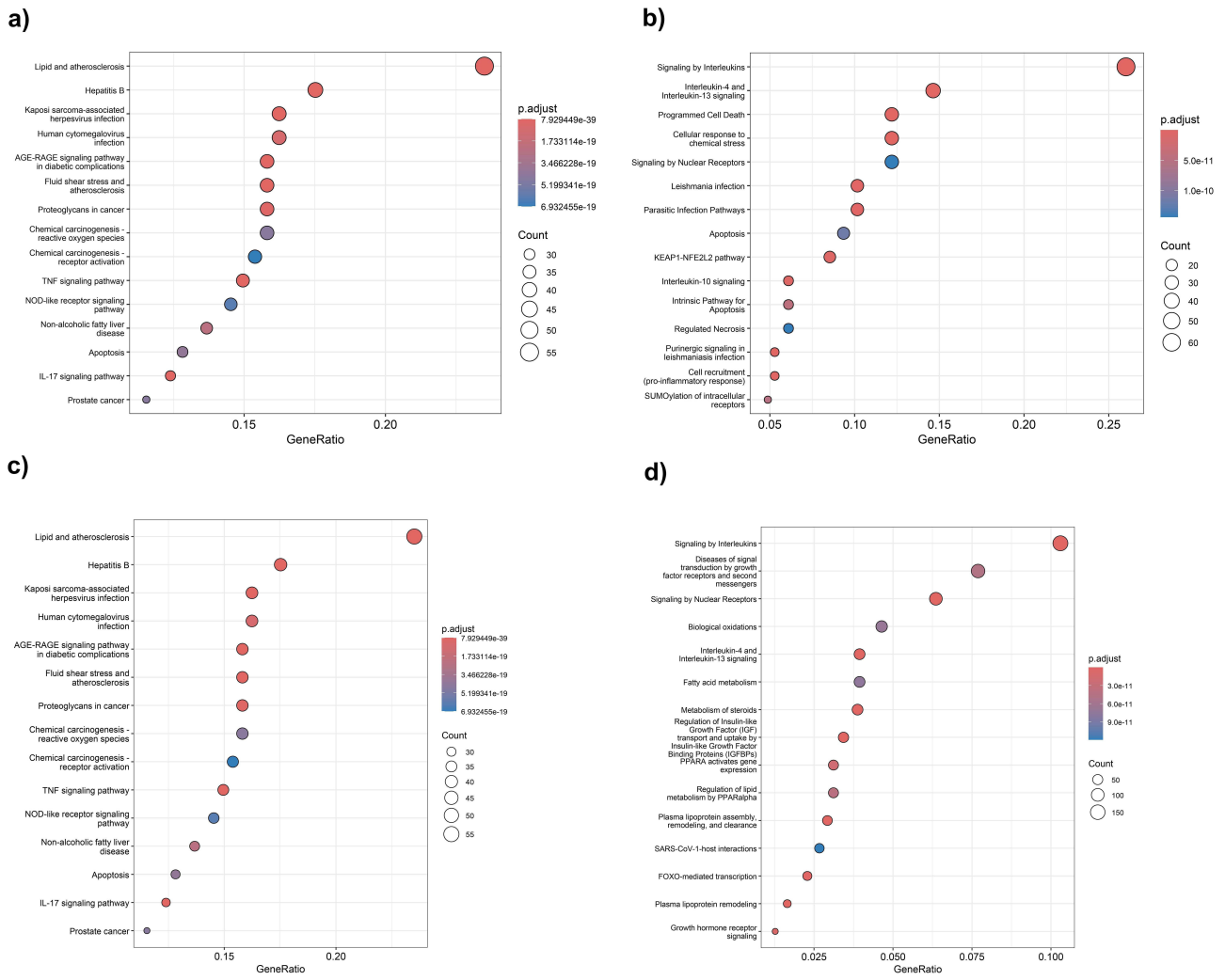

Figure 5 Pathway enrichment analysis. (**a**) KEGG pathway enrichment for shared proteins (andrographolide ∩ MAFLD). (**b**) KEGG pathway enrichment for MAFLD-related proteins (full MAFLD gene set). (**c**) Reactome pathway enrichment for shared proteins. (**d**) Reactome pathway enrichment for MAFLD-related proteins. The size of each dot represents the number of genes enriched in the pathway, and the color gradient indicates the adjusted p-value.

Cellular component analysis revealed a significant enrichment in the "vesicle lumen" (GO:0031983, $p=1.16\times10^{-18}$), "cytoplasmic vesicle lumen" (GO:0060205, $p=5.37\times10^{-18}$), and "secretory granule lumen" (GO:0034774, $p=2.22\times10^{-17}$). This suggests that andrographolide may influence secretory mechanisms and vesicle-mediated transport (Figure 6c).

Molecular Docking Analysis Reveals Strong Binding Affinity of Andrographolide to Key Protein Targets

Firstly, to validate the docking protocol, re-docking of the co-crystallized ligand (AZD5363, residue code 0XZ) into the crystal structure of AKT1 (PDB ID: 4GV1) was performed using the same parameters applied to the AlphaFold models. The re-docked pose showed close alignment with the crystallographic pose, with an RMSD of 1.109 Å (Figure 7a), which is below the accepted threshold of 2.0 Å. This confirms that the docking protocol can accurately reproduce known binding poses. Therefore, the same protocol was applied to the AlphaFold models of the ten hub proteins used in this study.

The information regarding protein targets sourced from the AlphaFold database is presented in Table 3. The parameters for the grid box corresponding to each target protein are detailed in Table 4. The dimensions of the grid varied from roughly 48×58 × 65 $Å^3$ for VEGFA to 142×129 × 118 $Å^3$ for EGFR, with the grid centers located at the geometric center of each respective protein (Table 4).

https://doi.org/10.2147/JEP.S625161

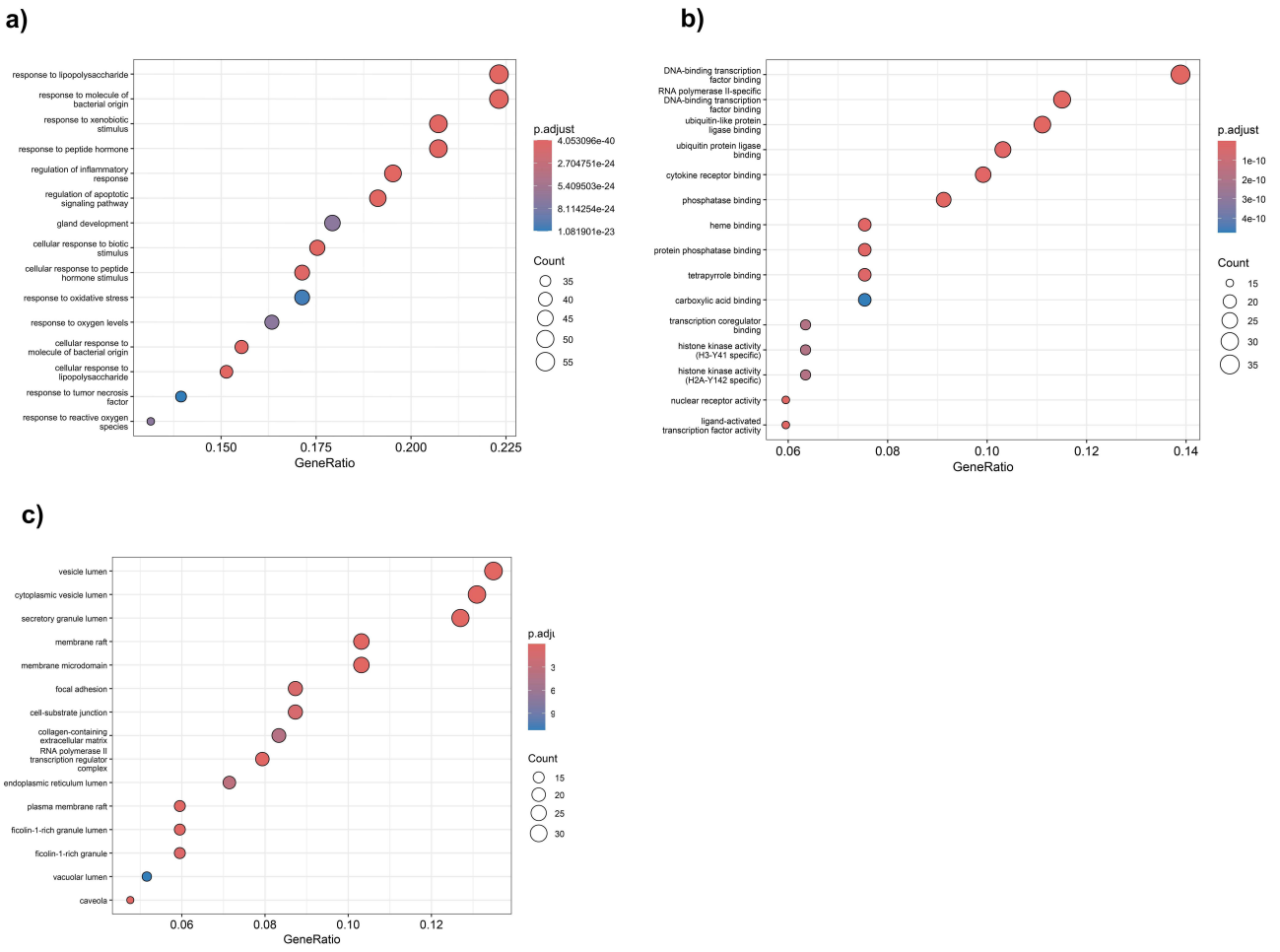

Figure 6 Ontology enrichment analysis. (**a**) Biological process. (**b**) Molecular function. (**c**) Cellular component. The size of each dot represents the number of genes enriched in the pathway, and the color gradient indicates the adjusted p value.

Molecular docking were conducted to assess the binding affinity and potential interactions between Andrographolide and a selection of ten proteins that play critical roles in the pathogenesis of MAFLD, encompassing inflammation, apoptosis, and insulin signaling pathways. The findings indicated that Andrographolide displayed strong binding energies below the threshold of −5.0 kcal/mol for all targets examined, signifying a high likelihood of spontaneous and stable binding. The binding energies calculated are summarized in Table 4. Importantly, Andrographolide demonstrated the highest binding affinity towards AKT1 (−7.7 kcal/mol), EGFR (−7.5 kcal/mol), and STAT3 (−7.2 kcal/mol), indicating its role as a high-affinity ligand for these essential signaling nodes.

Analysis of Hydrogen Bond Interactions Reveals Essential Binding Mechanisms

The detailed examination of the specific molecular interactions that stabilize the Andrographolide-protein complexes was conducted using Discovery Studio. This analysis concentrated on hydrogen bonds, which play a vital role in determining binding specificity and affinity. The principal interactions for each target are outlined below and compiled in Table 2. STAT3: The stability of the complex was attributed to five hydrogen bonds. Significant interactions included a side-chain interaction between Ser727 OG and its own backbone oxygen, as well as a backbone interaction between Arg729 N and Ser727 O. Additionally, the ligand (UNK1) established two direct hydrogen bonds with the protein, donating an H atom to the backbone oxygen of Met726. EGFR: The binding conformation was defined by four hydrogen bonds. Key interactions were noted between the backbone of Met54 and the side chain of Arg309. The ligand itself was involved in two bonds: one by donating an H atom to the backbone oxygen of Arg53 and another internal interaction. TP53: The

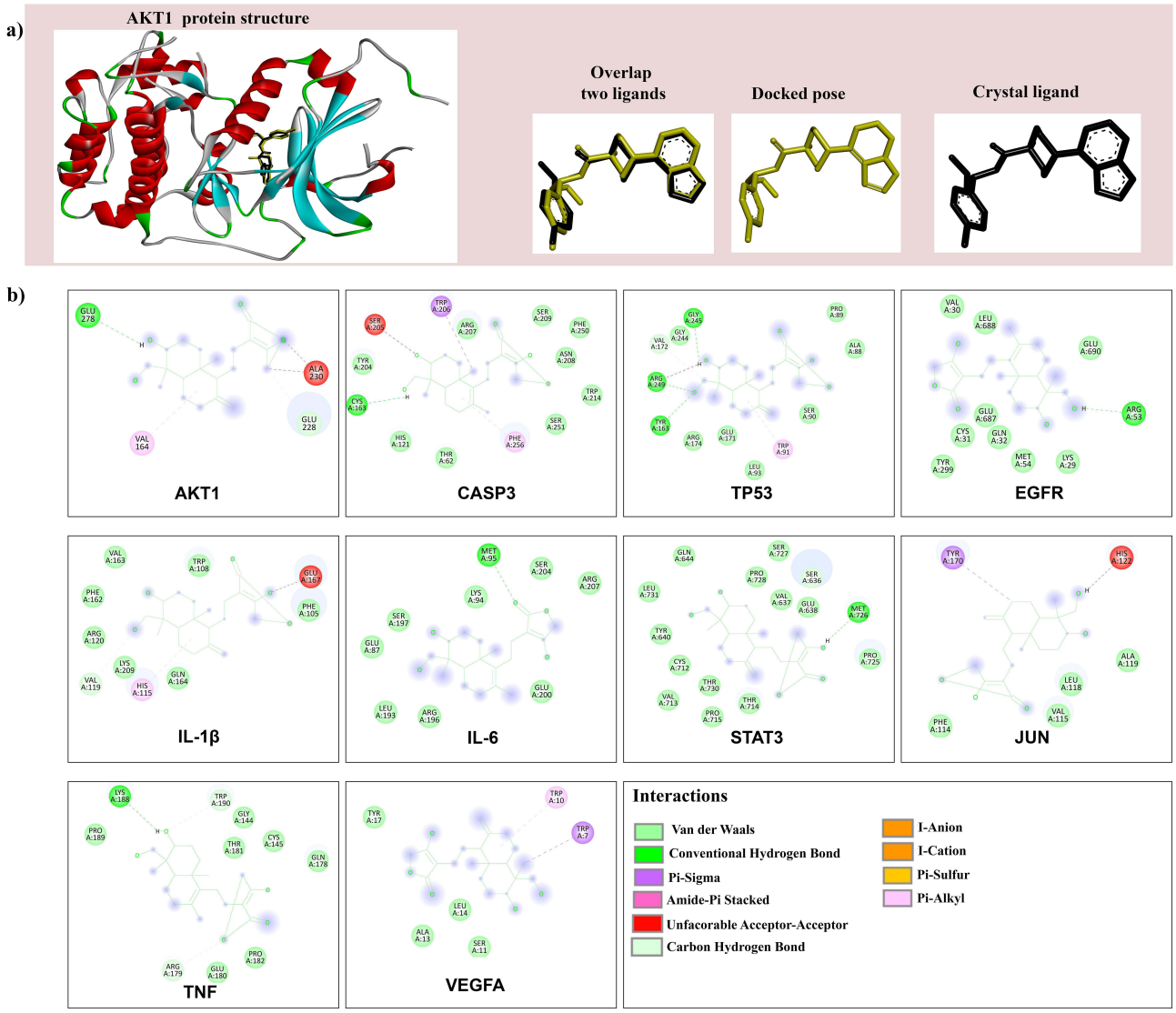

Figure 7 (**a**) Redocking validation of the docking protocol using AKT1 (PDB: 4GV1). Overlay of the crystallographic pose (black) and redocked pose (yellow) of AZD5363 (residue code 0XZ). The protein is shown as a cartoon representation. (**b**) Detailed bond interactions for each Andrographolide protein complex.

complex with the tumor suppressor p53 was stabilized by seven hydrogen bonds. A notably strong interaction was detected between Arg249 NH1 and Glu171 OE2 (2.65 Å). The ligand also established a direct bond with the tyrosine residue (Tyr163 OH). IL-6: Andrographolide formed a comprehensive network of seven hydrogen bonds with IL-6. Remarkably, a very short, strong bond (1.95 Å) was formed between Arg196 HH21 and Glu83 OE2, suggestive of a salt bridge. The ligand interacted directly with the protein through Ser204 HG and the side chain of Arg196. IL-1β: The stabilization of the binding was achieved through two classical backbone hydrogen bonds formed between Arg120 N and Val163 N with the backbone oxygens of Pro118 and Pro173, respectively. TNF: The complex exhibited five hydrogen bonds, predominantly involving the backbone atoms of the protein (Gly144, Cys145, Lys188, Trp190). Additionally, the ligand established one direct hydrogen bond within the binding pocket. JUN (Transcription Factor AP-1): A total of five hydrogen bonds were identified. His122 was highlighted as a crucial residue, with its ND1 atom forming two bonds with the ligand. Furthermore, the ligand also created an internal hydrogen bond. CASP3: Although only two hydrogen bonds were noted, one of these was a strong internal interaction within the ligand (2.33 Å), which likely plays a significant role in maintaining the stability of the bound conformation. VEGFA: The binding process was enhanced by two backbone-to-backbone hydrogen bonds from Ser11 N and Leu14 N to the oxygens of Trp7 and Trp10, respectively. AKT1: The

https://doi.org/10.2147/JEP.S625161

Table 3 Details of Protein Targets of MAFLD Selected for Molecular Docking with Andrographolide

Protein Target	Identifier	Method	Average pLDDT	Positions
TNF	AF-P01375-F1	AlphaFold	84.84	1–233
IL6	AF-P05231-F1	AlphaFold	85.23	1–212
AKT1	AF-P31749-F1	AlphaFold	82.34	1–480
TP53	AF-P04637-F1	AlphaFold	74.33	1–393
IL1B	AF-P01584-F1	AlphaFold	75.91	1–269
JUN	AF-P05412-F1	AlphaFold	61.07	1–331
VEGFA	AF-P15692-F1	AlphaFold	78.23	1–232
STAT3	AF-P40763-F1	AlphaFold	84.82	1–770
CASP3	AF-P42574-F1	AlphaFold	85.5	1–277
EGFR	AF-P00533-F1	AlphaFold	76.18	1–1210

Abbreviation: pLDDT, predicted Local Distance Difference Test score.

Table 4 Grid Box Parameters, Exhaustiveness Settings, and Predicted Binding Affinities of Andrographolide with Ten MAFLD-Associated Protein Targets

Protein	Grid Size (x, y, z)	Binding Energy (kcal/mol)	RMSD/ub Range (Å)	RMSD/lb Range (Å)
AKT1	(96.92, 84.20, 79.42)	**−7.7**	0 to 45.9	0 to 42.9
EGFR	(142.34, 128.88, 118.10)	**−7.5**	0 to 35.9	0 to 33.0
STAT3	(110.79, 97.96, 132.44)	**−7.2**	0 to 45.1	0 to 42.8
TP53	(86.35, 107.20, 84.92)	−6.9	0 to 35.6	0 to 33.3
CASP3	(127.27, 61.83, 79.99)	−6.9	0 to 9.34	0 to 4.54
IL1B	(101.44, 83.54, 119.78)	−6.7	0 to 30.5	0 to 28.2
IL6	(80.33, 78.50, 60.25)	−6.1	0 to 25.8	0 to 22.0
TNF	(98.56, 92.50, 112.93)	−5.8	0 to 30.5	0 to 27.3
VEGFA	(58.27, 48.49, 64.80)	−5.8	0 to 26.8	0 to 25.0
JUN	(88.06, 101.80, 117.01)	−5.3	0 to 39.9	0 to 35.6

Notes: Binding energies are in kcal/mol. RMSD/ub = upper bound RMSD (unconstrained), RMSD/lb = lower bound RMSD (constrained). The lowest binding energy (most favorable) for each target is shown. RMSD ranges represent the minimum (0, always the best pose) to maximum values across all 9 predicted binding modes. Bold indicates the strongest predicted binding affinity in comparison other targets.

interaction with AKT1 was particularly remarkable due to two salt bridge interactions between the positively charged Lys179 NZ and the negatively charged residues Glu198 OE1 and Asp292 OD1, with distances measuring 2.74 Å and 2.81 Å, respectively. A summary of Hydrogen bond interactions is presented in Table 5 and Figure 7b. This indicates a strong electrostatic influence on the binding mechanism.

Table 5 Hydrogen Bond Interactions Between Andrographolide and Key Protein Targets

Target Protein	Donor Atom (Residue)	Acceptor Atom (Residue/Ligand)	Distance (Å)	Coordinate (X, Y, Z)
AKT1	NZ (:LYS179)	OE1 (:GLU198)	2.74	−7.80, −3.17, 8.47
	NZ (:LYS179)	OD1 (:ASP292)	2.81	−5.82, −3.71, 8.26
	N (:ALA230)	O (Andrographolide)	3.05	−8.72, −12.99, 0.91
TP53	OH (:TYR163)	O (Andrographolide)	2.76	5.12, −4.67, −8.06
	NH1 (:ARG249)	OE2 (:GLU171)	2.65	4.63, −6.82, −11.93
	NH2 (:ARG249)	O (Andrographolide)	3.05	6.97, −5.37, −10.16
CASP3	H (Andrographolide)	O (Andrographolide)	**2.33**	12.06, 4.12, −11.17
EGFR	H (Andrographolide)	O (:ARG53)	**2.28**	−18.37, −1.75, 11.81
	H (Andrographolide)	O (Andrographolide)	**2.12**	−17.87, −1.51, 10.27

(*Continued*)

Table 5 (Continued).

Target Protein	Donor Atom (Residue)	Acceptor Atom (Residue/Ligand)	Distance (Å)	Coordinate (X, Y, Z)
IL-6	HH21 (:ARG196)	OE2 (:GLU83)	**1.95**	−18.59, 10.45, −2.38
	HH22 (:ARG196)	O (Andrographolide)	**2.24**	−15.14, 10.56, −2.64
	HG (:SER204)	O (Andrographolide)	**2.04**	−9.50, 6.19, −12.26
	HG (:SER204)	O (Andrographolide)	**2.14**	−8.65, 6.24, −11.52
	H (Andrographolide)	OE1 (:GLU87)	**2.36**	−13.40, 13.05, −2.55
STAT3	H (Andrographolide)	O (:MET726)	**2.02**	23.34, 15.89, −34.79
	H (Andrographolide)	O (Andrographolide)	**2.00**	17.33, 11.85, −37.16
	H (Andrographolide)	O (Andrographolide)	**2.26**	16.78, 11.52, −37.62
JUN	ND1 (:HIS122)	O (Andrographolide)	3.06	25.09, 20.61, 7.21
	ND1 (:HIS122)	O (Andrographolide)	2.90	25.33, 20.40, 5.87
	H (Andrographolide)	O (Andrographolide)	**2.32**	25.86, 19.80, 6.55
TNF	H (Andrographolide)	O (Andrographolide)	**2.30**	4.94, 7.15, −23.14

Notes: The table lists all identified hydrogen bond interactions with a distance of less than 3.2 Å. The donor and acceptor atoms are specified by the residue name and atom type. Internal ligand H-bonds are included as they influence the binding conformation. Coordinates (in Ångströms) represent the spatial midpoint of the hydrogen bond. Bold values in the Distance column indicate hydrogen bonds with the shortest distances (< 2.5 Å), representing the strongest hydrogen bond interactions. IL-1β and VEGFA had no specific ligand-protein H-bonds identified.

Oil Red O Staining Results

To assess the impact of andrographolide on OA-induced steatosis both visually and quantitatively, we conducted Oil Red O staining. The representative microscopic images (Figure 8a) revealed that control cells had minimal lipid droplet accumulation, while treatment with 1 mM OA for 24 hours significantly increased the number and intensity of red-stained lipid droplets within the cells. The quantitative assessment of Oil Red O staining indicated that 1 mM OA treatment significantly increased intracellular lipid levels when compared to the untreated control cells. The group treated with OA showed a mean absorbance of 2.07 ± 0.09 (95% CI: 1.69 to 2.45), reflecting a 186% increase in comparison to the control group, which had a mean absorbance of 0.72 ± 0.07 (95% CI: 0.44 to 1.01). This observed difference was statistically significant ($t(4) = 12.13$, $p = 0.0003$) and indicated an exceptionally large effect size (Cohen's $d = 9.91$, 95% CI: 2.86 to 16.96) (Figure 8).

Furthermore, co-treatment with 14 μM andrographolide resulted in a significant reduction of lipid accumulation caused by OA. The OA+Andrographolide group exhibited a mean absorbance of 1.29 ± 0.09 (95% CI: 0.92 to 1.66), which was 38% lower than the absorbance recorded in the OA-only group. Statistical analysis validated that this reduction was significant ($t(4) = -6.32$, $p = 0.0032$) with a very large effect size (Cohen's $d = -5.16$, 95% CI: −9.07 to −1.24) (Figure 8).

Real-Time Validation in Steatotic Hepatocytes

Quantitative real-time PCR analysis showed that when andrographolide was co-administered, there was a significant decrease in the mRNA expression levels of AKT1, EGFR, and STAT3 in OA-induced steatotic HUH7 hepatocytes (Figure 9). Compared to cells treated only with OA, all three genes displayed considerable downregulation. These alterations in transcript levels imply that treatment with andrographolide may influence these signaling pathways. However, it remains unclear whether this effect is due to direct transcriptional regulation or if it is a secondary result of decreased lipid accumulation and cellular stress, as mRNA data alone cannot provide a definitive answer.

The analysis of GAPDH expression stability across treatment groups indicated that the Cq values for GAPDH did not show significant differences between the experimental groups ($p > 0.05$). This supports the use of GAPDH as a stable reference gene for qRT-PCR normalization under our experimental conditions. The ΔCT values for AKT1 rose from 2.26 ± 0.31 in OA-treated cells to 4.18 ± 0.29 in cells treated with OA and Andrographolide, reflecting a 1.91-unit increase in ΔCT ($t(4) = -4.02$, $p = 0.0159$). This translates to a 0.27-fold decrease in AKT1 expression (95% CI: 0.11–0.66), which corresponds to a 73.5% reduction (Table 3). In the case of EGFR, ΔCT values increased from 3.05 ± 0.34 to 4.89 ± 0.26 ($\Delta\Delta CT = 1.84$, $t(4) = -4.20$, $p = 0.0137$), leading to a 0.28-fold reduction (95% CI: 0.12–0.65) or a 72.0% decrease in expression. STAT3 exhibited the least significant down-regulation, with ΔCT values increasing from 2.67 ± 0.28 to 3.78 ± 0.25 ($\Delta\Delta CT = 1.11$, $t(4) = -3.64$, $p = 0.0220$), indicating a 0.46-fold reduction (95% CI: 0.26–0.83) or a 53.6% decrease in expression (Figure 9).

https://doi.org/10.2147/JEP.S625161

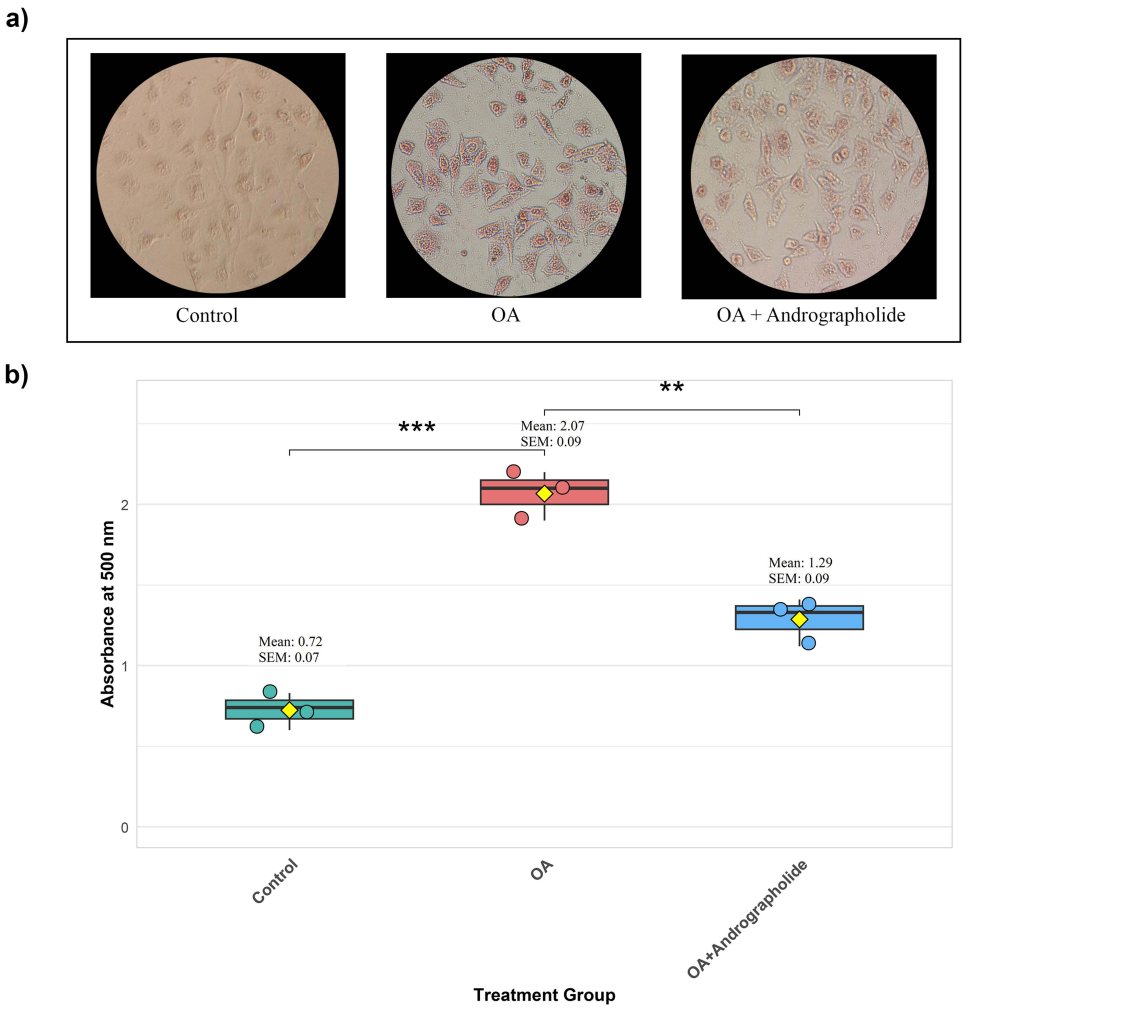

Figure 8 The protective effect of Andrographolide against OA-induced lipid accumulation in HUH7 cells after 24 hours of treatment. (**a**) Representative microscopic images of Oil Red O staining for the control, OA-only (1 mM), and OA + Andrographolide (14 μM) groups (Light microscope at 40× magnification). (**b**) Quantitative analysis of intracellular lipid content measured by spectrophotometric absorbance at OD 500 nm. Data are expressed as mean ± SEM from three independent experiments. Statistical significance was determined using Student's *t*-test; **p < 0.01, ***p < 0.001. Yellow diamonds represent individual group mean values.

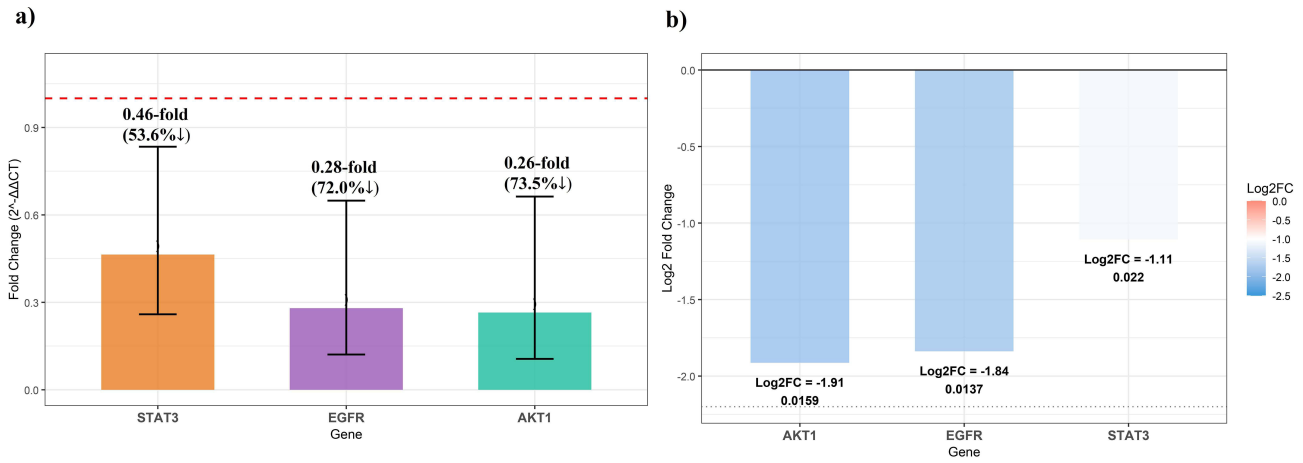

Figure 9 Andrographolide differentially modulates the expression of signaling molecules in steatotic hepatocytes. (**a**) Relative fold change ($2^{-\Delta\Delta CT}$) in mRNA expression of target genes in OA-induced HUH7 hepatocytes treated with andrographolide, normalized to the OA-only control (red dashed line, Fold Change = 1.0). Data are presented as mean fold change with 95% confidence intervals (error bars) from three independent experiments. Percent reduction in gene expression is indicated above each bar. ↓ indicates decreased fold change (**b**) Log2Fold Change values for each target gene. Negative values denote downregulation following andrographolide co-administration. P-values were derived from Student's *t*-test.

Discussion

Our comprehensive multi-methodology strategy, which integrates computational systems pharmacology with experimental validation, offers substantial evidence regarding the therapeutic efficacy of andrographolide in the context of MAFLD. The foundational computational framework established a solid molecular basis, demonstrating a 32.11% overlap between the targets of andrographolide and proteins associated with MAFLD, while also identifying critical hub genes (TNF, IL6, AKT1, TP53, IL1B, JUN, VEGFA, STAT3, CASP3, and EGFR) within a highly interconnected network. Importantly, these in silico predictions were corroborated by our in vitro results. Co-treatment with andrographolide significantly reduced OA-induced lipid accumulation in HUH7 hepatocytes by 38%, illustrating its direct antisteatotic properties. Additionally, qPCR analysis validated the modulation of key hub genes, revealing that andrographolide significantly downregulated the expression of AKT1, EGFR, and STAT3 mRNA in the steatotic model. While these findings at the transcript level show a correlation, they do not actually prove that there's a direct inhibition of the protein functions of AKT1, EGFR, or STAT3. To really understand the mechanisms at play, we need to validate these results at the protein level, especially by looking at the phosphorylation-specific activity of AKT1 and STAT3. The alignment of computational predictions with experimental findings strongly indicates that the therapeutic potential of andrographolide stems from its multi-target nature, effectively addressing the interconnected pathological processes of dysregulated metabolism, inflammation, and insulin signaling that are characteristic of MAFLD.

Our computational analysis indicates that andrographolide (MW 350.45, C_20H_30O_5) exhibits generally positive drug-like characteristics. It adheres to Lipinski's rule of five (no violations), demonstrating moderate lipophilicity (cLogP ≈2.5) and a high proportion of sp^3 carbons (Fsp^3 ≈0.75). These attributes are often associated with favorable oral bioavailability. Nevertheless, the predicted aqueous solubility is low (LogS ≈–4.3), which aligns with the established poor water solubility of andrographolide (logP≈2.63) and the low bioavailability documented in the literature.[45,46] For instance, Ye et al (2011) highlighted andrographolide's "poor oral bioavailability" attributed to its low solubility and rapid metabolism.[45] Although its rigid conformation (with only 3 rotatable bonds) and moderate polar surface area (PSA of 86.99 $Å^2$) are conducive to permeability, the low solubility likely restricts absorption. Indeed, formulation studies underscore that andrographolide's "poor solubility (logP≈2.6) and low oral bioavailability" necessitate solubilizing strategies.[46] The various bioactivities of andrographolide encompass anti-inflammatory, antibacterial, hepatoprotective, and other well-established effects.[47] However, its inadequate pharmacokinetics pose a significant obstacle to its clinical application. Patil and Jain (2021) provided a thorough review of analytical techniques, including chromatography and spectrophotometry, which are vital for quantifying this compound in biological matrices and formulations, highlighting the necessity for stringent quality control in any delivery method.[47] In conclusion, while the size and polarity of andrographolide align with drug-likeness, its solubility and dispersion pose significant challenges.

Andrographolide's anticipated ADME profile reveals challenges in absorption and distribution. Both in silico Caco-2 and MDCK models demonstrate extremely low apparent permeability ($<10^{-5}$ cm/s), alongside a significant likelihood of P-glycoprotein (P-gp) efflux (substrate probability ≈0.009). These forecasts are consistent with experimental pharmacokinetic data. Panossian et al (2000) noted that when administered orally to rats, andrographolide was "rapidly and nearly completely absorbed," yet its bioavailability significantly decreased at elevated doses.[48] They attributed this dose-dependent behavior to substantial first-pass metabolism and moderate plasma protein binding (~55%). Similarly, Ye et al (2011) reported that the absolute oral bioavailability of andrographolide in rats was merely ~2.7%; the compound underwent rapid metabolism (eg, conversion to a 14-sulfonate conjugate) in the gastrointestinal tract and liver, exhibiting four-fold greater permeability in the basolateral to apical direction in vitro, indicative of active efflux. In situ perfusion studies confirmed that the inhibition of P-gp by verapamil markedly enhanced the jejunal/ileal uptake of andrographolide.[45] Therefore, our in-silico observations of poor Caco-2/MDCK permeation and P-gp substrate characteristics are corroborated by these experimental findings: the absorption of andrographolide is constrained by both metabolic processes and efflux mechanisms, resulting in minimal systemic exposure following oral administration. The intersection of these bioavailability issues with the compound's promising therapeutic potential has spurred the development of innovative delivery methods. Recently, Peng et al (2026) demonstrated that encapsulating andrographolide within exosome-like nanoparticles (ELNs) derived from Nauclea officinalis markedly improved its anti-NASH efficacy

in WRL68 cells, surpassing both the free drug and unloaded ELNs. This formulation effectively tackled the poor solubility and short half-life identified in our analysis, and the synergistic effect combining the anti-inflammatory and antioxidant properties of andrographolide with miRNA-mediated metabolic regulation by ELNs, reinforces the justification for nanoparticle-based strategies to address the absorption challenges we anticipated. Furthermore, the study validated that such formulations can diminish pro-inflammatory cytokines and lipid accumulation, confirming that the therapeutic potential of the compound can be realized when its solubility and bioavailability are enhanced.[28]

Predicted distribution parameters imply moderate tissue penetration. A volume of distribution (Vd_SS ≈ –0.30 L/kg) and a calculated unbound fraction (Fu ≈ 33.8%) suggest that a limited proportion circulates freely in plasma. This aligns closely with the ~45% unbound fraction (55% protein-bound) reported by Panossian et al[48] The anticipated low permeability across the blood–brain barrier (BBB probability ≈0.28) is also reasonable, considering the pronounced P-gp efflux and restricted lipophilicity, indicating that andrographolide may not easily penetrate the central nervous system.

Andrographolide is anticipated to be a non-inhibitor of the primary human CYP enzymes, indicating a low likelihood of CYP-mediated drug–drug interactions. This observation is consistent with existing literature: Ye et al reported rapid metabolism by the gut and liver (S9 fraction) but did not indicate any inhibitory effects on CYPs.[45] The renal excretion of the unchanged drug is minimal; the majority of clearance seems to be metabolic, as no significant parent compound was detected in urine during animal studies.[48]

The computational toxicity assessment produced mixed results. The estimated acute oral LD_{50} (approximately 1890 mg/kg in rats) categorizes andrographolide in GHS category 4 ("harmful if swallowed"), which aligns with pharmacological safety thresholds. In contrast, a standardized Andrographis extract (which contains andrographolide) exhibited no adverse effects even at doses of 5000 mg/kg in rats,[49] implying that the actual acute toxicity is low.

More alarming are the elevated probabilities for carcinogenicity (0.98) and genotoxicity (0.99) identified by one model. However, these in-silico warnings are at odds with experimental findings. Sharifuddin et al (2012) evaluated pure andrographolide in human lymphoblastoid cells and observed no significant genotoxicity (micronucleus formation did not exceed the control range).[50] Likewise, an Ames test conducted on an A. paniculata extract (KalmCold) returned negative results for mutagenicity.[49] Therefore, while our computational models raised a flag of caution, published in vitro research suggests that andrographolide is not mutagenic under the conditions tested. Nonetheless, the predictions necessitate caution and imply that additional in vivo carcinogenicity studies would be advisable.

The anticipated organ-specific toxicities for the liver and kidneys were predominantly benign: high probabilities of inactivity were noted for hepatotoxicity (P≈0.93) and nephrotoxicity (P≈0.51). In fact, andrographolide is widely regarded as hepatoprotective across various models,[23] rather than hepatotoxic. The likelihood of hERG blockade (QT prolongation) was assessed to be low (P≈0.22), and experimental findings do not indicate any cardiotoxic effects associated with andrographolide. Our model did identify moderate immunotoxicity (P≈0.82) and cardiotoxicity (P≈0.55). There are no direct reports of immune or cardiac adverse effects from andrographolide in vivo; rather, it is more commonly recognized for its immunomodulatory and anti-inflammatory properties.[51] Therefore, these predictions should be approached with caution.

Our in vitro discovery that andrographolide markedly diminishes OA-induced lipid accumulation in HUH7 hepatocytes offers direct cellular validation of its anti-steatotic properties, which are fundamental to MAFLD treatment. The recorded 38% decrease in lipid content is strongly supported by the existing body of evidence from both cellular and animal studies. For example, Ran et al (2023) illustrated that andrographolide mitigated hepatic steatosis in mice fed a HFD and decreased lipid droplets in OA-treated LO2 cells, mechanistically associating this effect with the inhibition of fatty acid uptake through the downregulation of Fatty Acid Transport Protein 2 (FATP2).[19] Our findings complement this by validating the effectiveness of andrographolide in a distinct hepatoma cell line (HUH7), thereby reinforcing the reproducibility of its lipid-lowering impact across various experimental frameworks. Likewise, Pipitone et al (2023) indicated that andrographolide, both independently and in conjunction with curcumin, effectively reduced triglyceride levels and reactive oxygen species (ROS) in steatotic HepG2 cells.[2] Our quantitative Oil Red O analysis provides further detail to these findings, offering a precise quantification of the effect size (Cohen's d = −5.16).

The anti-lipid activity we observed aligns with findings from other cellular models. Chen et al (2016) illustrated that andrographolide inhibited adipogenesis in 3T3-L1 cells by downregulating C/EBPβ expression and its phosphorylation, which in turn diminished the expression of C/EBPα and PPARγ, leading to a reduction in lipid accumulation.[20] In

a similar vein, Kaewkittikhun et al (2021) reported that andrographolide decreased lipid droplet accumulation in adipocytes derived from human bone marrow mesenchymal stem cells by inhibiting adipogenic regulators.[21] These results, in conjunction with our own, suggest that andrographolide exerts anti-lipogenic effects across various cell types and species, indicating a conserved mechanism that likely underpins its hepatoprotective properties.

Moreover, the significant reduction corresponds with in vivo results from Cabrera et al (2017) and Hu et al (2025), where the administration of andrographolide led to decreased hepatic triglyceride levels and improved histological steatosis in dietary rodent models of MASH and MAFLD, respectively.[52,53] This alignment between our simplified in vitro model and the intricate in vivo pathophysiology enhances the translational significance of andrographolide's anti-lipogenic effects.

The hepatoprotective capabilities of andrographolide extend beyond the realm of lipid metabolism. Abdulaziz Bardi et al (2014) demonstrated that Andrographis paniculata leaf extract mitigated thioacetamide-induced liver cirrhosis in rats, leading to a reduction in fibrosis, lymphocyte infiltration, and oxidative stress, while also restoring serum liver biomarkers.[25] Lin et al (2018) further established that andrographolide improved CCl_4-induced liver fibrosis in mice by inhibiting the TLR4/NF-κB and TGF-β1/Smad2 signaling pathways.[54] Yan et al (2018) found that andrographolide lessened APAP-induced liver fibrosis through the activation of the Nrf2 antioxidant pathway.[17] More recently, Zhang et al (2025) revealed that andrographolide mitigates acute liver injury by inhibiting the NLRP3/Caspase-1/GSDMD-mediated pyroptosis pathway,[34] while Li et al (2026) discovered that it alleviates Salmonella-induced liver damage in mice by suppressing PANoptosis.[55] Taken together, these studies reinforce our findings and establish andrographolide as a multi-target hepatoprotective agent with effects on steatosis, inflammation, fibrosis, and cell death pathways.

Overall, the in-silico toxicity profile indicates that the compound is relatively safe, with the exception of potential false-positive signals for genotoxicity. Importantly, all significant CYP450 and nuclear receptor pathways (Tox21 assays) were predicted to be inactive (probabilities >0.77–0.99), suggesting a minimal risk of andrographolide inducing drug–drug interactions through metabolic inhibition. This aligns with the absence of reported CYP inhibition by andrographolide in existing literature.

Our analysis of network pharmacology has revealed 10 hub genes that lie at the intersection of the targets of andrographolide and proteins associated with MAFLD: TNF, IL6, AKT1, TP53, IL1B, JUN, VEGFA, STAT3, CASP3, and EGFR. These genes constitute a highly interconnected core involved in the regulation of inflammation and metabolism (Table 2). It is noteworthy that TNF, IL6, and IL1B are well-established pro-inflammatory cytokines that play a role in the pathogenesis of MAFLD/MASH.[56–59] STAT3 acts as the transcriptional effector for IL-6 signaling, while AKT1 serves as a pivotal node within the insulin/PI3K signaling pathway; both have been previously emphasized in the context of andrographolide's effects on metabolic disorders.[60,61] CASP3 (caspase-3) and TP53 are associated with apoptosis and stress responses, aligning with the pro-apoptotic properties of andrographolide in cancer cells.[62] Additionally, EGFR and JUN, a component of AP-1, function as hubs for growth factor signaling, whereas VEGFA is implicated in angiogenesis and also plays a role in modulating inflammation.

Crucially, similar hub targets have been documented in other contexts of MAFLD. Lei Li et al (2021) reported that the core predicted targets of andrographolide within a MASH network included TNF, IL6, IL1B, and AKT1, all of which are enriched in the MAFLD pathway.[61] This convergence indicates that andrographolide may exert its therapeutic effects by influencing the chronic inflammatory environment characteristic of MASH. Cabrera et al (2017) demonstrated that treatment with andrographolide in a mouse model of MASH resulted in significant reductions in hepatic inflammation and fibrosis, characterized by a "strong reduction in hepatic macrophage infiltration and decreased hepatic mRNA levels of pro-inflammatory and pro-fibrotic genes".[23] The hub genes we identified (TNF, IL6, IL1B) are likely responsible for these anti-inflammatory effects. For example, the ability of andrographolide to inhibit NF-κB is expected to suppress the production of IL-1β, TNF-α, and IL-6,[51,56,63–65] which corresponds with the downregulation observed in livers subjected to treatment.

The network is categorized into four primary modules (Figure 4). Community 3 encompasses pro-inflammatory cytokines and immune regulators (TNF, IL6, IL1B, chemokines, MMPs), which aligns with the inflammatory theme of Module 3. Community 1, focused on cell signaling and the cell cycle, includes STAT3, JUN, TP53, EGFR, and MAPKs, which are associated with proliferation and stress responses. Community 4, related to lipid metabolism and nuclear

receptors, contains PPARs and FABPs, indicating that andrographolide influences lipid management – a notion supported by recent findings (detailed below). Community 2, which pertains to metabolism and antioxidants, includes CYP450 enzymes and glutathione pathways, suggesting a role in modulating oxidative stress. In conclusion, the hub genes we identified are well-integrated with established MAFLD biology (inflammation, lipid dysregulation, cell death) and with the documented activities of andrographolide, highlighting its multi-target potential in liver disease.

The KEGG pathway analysis of the shared targets revealed several pathways pertinent to MAFLD. The "Lipid and Atherosclerosis" pathway emerged as the most enriched ($p \approx 7.9 \times 10^{-39}$), reflecting the lipid dysregulation characteristic of fatty liver. The classic MAFLD pathway itself (hsa04932) was significantly enriched ($p \approx 2.3 \times 10^{-19}$; involving 32 targets), emphasizing that numerous andrographolide targets are situated within pathways explicitly associated with fatty liver. The AGE-RAGE signaling pathway (hsa04933) and the Hepatitis B pathway (hsa05161) were also highly ranked. These findings are consistent with other research: Lei et al (2021) similarly observed that the targets of andrographolide are enriched in MAFLD signaling and fatty acid synthesis pathways.[61]

Reactome analysis indicated that interleukin signaling is a predominant theme. The terms "Signaling by Interleukins" and "IL-4 and IL-13 signaling" emerged as the most significant findings, aligning with the notable presence of IL6, IL1B, TNF, among others. Additionally, the concepts of "Programmed cell death" and "cellular response to chemical stress" were also enriched, connecting to processes of apoptosis and oxidative stress. These results are consistent with the established anti-inflammatory properties of andrographolide. For instance, andrographolide is known to significantly inhibit IL-6/STAT3 signaling[60] and to block NF-κB-dependent cytokine release.[58,64,65]

Gene Ontology (GO) enrichment analysis further elucidates the functional implications of our target set. Within the Biological Processes category, the terms "response to lipopolysaccharide" and "response to molecule of bacterial origin" were the most prominent ($p \approx 10^{-40}$). This underscores the activation pathways of the innate immune system; indeed, endotoxin (LPS) serves as a critical initiator of hepatic inflammation in MASH. The over-representation of andrographolide's targets among LPS-response genes suggests that it may mitigate inflammatory signals derived from the gut. Experimental evidence supports that andrographolide can inhibit LPS-induced inflammation (eg, in Kupffer cells) through NF-κB blockade.[23]

In terms of Molecular Function, the enrichment of "DNA-binding transcription factor binding" and "nuclear receptor activity" suggests that andrographolide may influence transcriptional regulators (eg, NF-κB, PPARs). Notably, PPAR-α/γ are present in our network (Community 4), and there are reports of andrographolide affecting PPAR signaling in metabolic disorders. The analysis of Cellular Component revealed terms such as "vesicle lumen" and "secretory granule lumen". These terms may indicate involvement in cytokine secretion or lipid transport vesicles. For example, IL-1β and IL-6 undergo processing in secretory vesicles; thus, andrographolide's interference in these pathways could modify cytokine release.[66] Overall, the GO and pathway profiles present a cohesive narrative: the target network of andrographolide is significantly oriented towards inflammation, particularly innate immune responses.

Our docking investigations offer molecular-level evidence supporting the multi-target effects of andrographolide. All ten selected proteins associated with MAFLD exhibited strong predicted binding affinities (all $\Delta G < -5$ kcal/mol), indicating potential physical interactions. Notably, the strongest affinities were observed with AKT1 (–7.7 kcal/mol), EGFR (–7.5 kcal/mol), and STAT3 (–7.2 kcal/mol), suggesting robust binding to critical signaling kinases. The significant binding to AKT1 is particularly noteworthy: AKT/PI3K signaling is known to regulate lipid synthesis and insulin responses in hepatocytes. Theoretical inhibition of AKT1 could lead to a decrease in lipogenesis. The significance of AKT inhibition in hepatic steatosis is robustly supported by in vivo genetic investigations. Wang et al (2021) illustrated that the simultaneous deletion of Akt2 and AMPKα2 in murine models provided resistance to obesity and hepatic steatosis induced by a high-fat diet. This effect was mediated by the preservation of Parkin-mediated mitophagy and the suppression of lipogenic genes such as FAS, SREBP1, PPARγ, and DGAT1. Notably, liver samples from obese individuals exhibited increased phosphorylation of Akt and FoxO1, thereby underscoring the clinical importance of Akt signaling in metabolic dysregulation. These results offer mechanistic validation for our docking predictions that andrographolide may exert anti-steatotic effects through the modulation of AKT, as the genetic ablation of Akt2 mirrors the lipid-lowering phenotype observed in vitro.[67]

Likewise, our substantial binding to EGFR corresponds with recent research indicating that andrographolide downregulates EGFR in cancer cells.[68] In a study focused on breast cancer, andrographolide was demonstrated to directly target EGFR, inhibiting epithelial-mesenchymal transition (EMT).[68] Considering EGFR's involvement in hepatocyte growth and regeneration, this interaction may influence liver proliferation or fibrosis.

The analysis of hydrogen-bond interactions identifies crucial residues within each complex. For instance, andrographolide established multiple hydrogen bonds with STAT3 (through Ser727 and Arg729 interactions) (Table 3). This finding aligns with existing literature, which indicates that andrographolide inhibits STAT3 phosphorylation and signaling in cancer cells.[60] The docking results imply that andrographolide fits into the STAT3 SH2 domain or an adjacent pocket, stabilized by five hydrogen bonds. In the case of EGFR, significant interactions included Met54 and Arg309 within the kinase domain, supporting the idea that andrographolide can bind to EGFR and hinder its activity.[68] Inhibition of EGFR may also play a role in diminishing liver fibrosis, as EGFR inhibitors have been shown to reduce stellate cell activation in MASH models.[69] Yin et al (2025) recently revealed that andrographolide influences the STAT3/PI3K/Akt pathway in diabetic nephropathy, leading to reductions in oxidative stress, inflammation, and apoptosis in podocytes. Utilizing network pharmacology, molecular docking, and in vivo validation, they identified STAT3, PI3K, and AKT1 as primary targets of andrographolide, with high binding affinities confirmed through molecular docking studies. Their research demonstrated that andrographolide markedly enhanced renal function and mitigated fibrosis by inhibiting the RAGE-NF-κB and STAT3/PI3K/Akt pathways.[35] These findings support our docking results and imply that the multitarget engagement of andrographolide with AKT1 and STAT3 may be fundamental to its extensive therapeutic effects across metabolic and inflammatory disorders, including MAFLD. The qPCR findings, indicating a notable downregulation of AKT1, EGFR, and STAT3 mRNA in steatotic hepatocytes, not only confirm but also enhance the forecasts derived from our network pharmacology analysis and docking investigations.

The binding to pro-inflammatory cytokines is particularly noteworthy. The docking analysis with IL-6 revealed the formation of five hydrogen bonds (for instance, a robust Arg196–Glu83 bond), indicating that andrographolide may stabilize itself on the surface of IL-6. This observation is significant as andrographolide is known for its anti-inflammatory properties, which include the reduction of IL-6 production;[70–72] direct binding could potentially disrupt the engagement of the IL-6 receptor. In a similar vein, the binding with TNF involved five hydrogen bonds (for example, at Gly144 and Cys145), suggesting that andrographolide may interact with TNF-α. Although this remains speculative, such binding could influence TNF signaling.

The interaction with caspase-3 (CASP3), despite exhibiting only two hydrogen bonds, was sufficiently strong ($\Delta G \approx -6.9$ kcal/mol) to imply the formation of a stable complex. This aligns with findings that andrographolide promotes caspase-3-mediated apoptosis in various cell types.[62] By binding to CASP3, andrographolide may allosterically enhance its activation or simulate a substrate. In osteosarcoma cells, andrographolide has been demonstrated to "significantly induce caspase-3, −8, and −9 activation, resulting in PARP cleavage",[62] which is consistent with our docking results supporting a direct interaction with CASP3.

The docking findings with transcriptional regulators TP53 (–6.9 kcal/mol) and JUN (–5.3 kcal/mol) indicate potential anti-tumor effects. Although p53 is frequently mutated in various diseases, andrographolide has been reported to degrade mutant p53 and to induce apoptosis independent of p53.[73] In this context, andrographolide forms seven hydrogen bonds with wild-type p53 (involving Arg249 and Tyr163), which may affect the activity or stability of p53. The binding of JUN (with multiple bonds to His122) could modulate the activity of the AP-1 transcription factor; andrographolide has been noted to influence c-Jun levels in the context of lung inflammation.[74] The interaction with TP53 holds significant importance in the context of hepatocyte senescence, a phenomenon that is increasingly acknowledged in the development of fatty liver disease. Qi et al (2022) illustrated that the suppression of hepatocyte senescence, marked by a reduction in senescence-associated β-galactosidase activity and a decrease in the expression of p16 and p21, effectively improved alcoholic fatty liver disease (AFLD) in mice subjected to ethanol and in ethanol-treated LO2 cells.[75] Importantly, p53 serves as a principal regulator of cellular senescence through its transcriptional regulation of p21, while the senescence-associated secretory phenotype (SASP) plays a role in promoting liver inflammation and fibrosis. Although Qi et al (2022) focused on curcumol instead of andrographolide, their results indicate that targeting pathways related to p53-induced senescence can provide substantial hepatoprotection against steatotic damage.[75] Our docking predictions suggest

a strong binding affinity of andrographolide to TP53, indicating that andrographolide may also influence hepatocyte senescence, thereby enhancing its direct anti-lipogenic effects. This proposition is further supported by the extensive anti-inflammatory and antioxidant characteristics of andrographolide, which may affect the senescence-associated secretory phenotype and the inflammatory environment within the steatotic liver.

Ultimately, the binding of VEGFA (–5.8 kcal/mol) involved interactions with the backbone; although andrographolide is not primarily recognized for its anti-angiogenic properties, VEGFA plays a role in fibrosis and inflammation associated with MASH,[76] thus modulation in this context cannot be dismissed. In summary, the docking and interaction patterns are biologically credible and enhance the network analysis. The anticipated strong affinity for STAT3, EGFR, AKT1, CASP3, IL-6, and TNF aligns with the documented effects of andrographolide (anti-inflammatory, pro-apoptotic) and underscores its polypharmacological nature.

It is crucial to emphasize that the anticipated binding energies, especially those around −5.8 kcal/mol (eg, TNF, VEGFA) and −5.3 kcal/mol (JUN), indicate relatively moderate interactions and should not be construed as definitive proof of biologically significant binding. Even the most robust predicted interactions (−7.7 kcal/mol for AKT1) necessitate experimental confirmation. These computational forecasts function as a prioritization mechanism to inform subsequent experimental investigations rather than serving as conclusive proof of therapeutic effectiveness.

By synthesizing all findings, andrographolide is revealed as a structurally "drug-like" compound with multi-target pharmacological properties, albeit with pharmacokinetic challenges. Its limited solubility and significant efflux suggest that reaching therapeutic levels in the liver may prove difficult without specific formulation strategies. In fact, recent research has introduced nanocrystal formulations aimed at enhancing the bioavailability of andrographolide.[45] Nevertheless, once administered, andrographolide seems ready to interact with critical pathways related to MAFLD. Our enriched pathways (lipid metabolism, IL signaling, NF-κB-related inflammation) correspond with in vivo observations: for instance, Ran et al (2022) demonstrated that andrographolide dose-dependently mitigated hepatic steatosis in mice fed a high-fat diet, primarily by inhibiting FATP2-mediated fatty acid uptake.[19] This innovative mechanism complements our network predictions: while FATP2 was not included in our target list, the broader pathway of fatty acid uptake and triglyceride synthesis (the "lipid and atherosclerosis" KEGG pathway) is prominently emphasized in our analysis, reinforcing Ran's finding that andrographolide diminishes liver lipid accumulation by restricting fatty acid transport.[19]

Furthermore, the inhibitory effect of andrographolide on inflammatory signaling is well documented. Cabrera et al (2017) demonstrated that andrographolide diminished hepatic macrophage infiltration and reduced the expression of IL-1β, TNF-α, and other cytokines in MASH mice.[23] The focus of our network on TNF, IL6, IL1B, STAT3, and others aligns with this: andrographolide likely disrupts the detrimental cycle of LPS/Kupffer cell activation leading to NF-κB/STAT3 signaling and subsequent cytokine release. Indeed, the study indicated that NF-κB inhibition is a probable mechanism,[23] which is consistent with docking studies showing that andrographolide interacts with proteins (such as STAT3 and IL-6) involved in these pathways.

Several limitations of this study warrant consideration. These experimental results are aligned with our computational predictions and indicate that treatment with andrographolide influences these signaling pathways. However, it's crucial to recognize that changes in mRNA might be secondary effects stemming from decreased cellular steatosis and enhanced metabolic health, rather than direct changes in transcription. Therefore, although our integrated computational and mRNA expression data suggest these pathways play a role in the anti-steatotic effects of andrographolide, they do not confirm a direct causal relationship. Additional, our integrated approach, combining gene expression analysis with molecular docking, offers a detailed framework for exploring how andrographolide might work. The predictions from molecular docking indicate possible direct interactions with important proteins, and the mRNA expression data show that these pathways are influenced during the anti-steatotic response. However, since the changes in mRNA are correlative and the docking predictions are based on computational models, we should view these results as generating hypotheses rather than providing definitive proof of mechanisms. While our qRT-PCR data demonstrate significant downregulation of AKT1, EGFR, and STAT3 mRNA in response to andrographolide treatment, mRNA changes cannot confirm direct inhibition of the encoded proteins. Therefore, the transcript-level changes reported in this study are correlative observations and should not be interpreted as evidence of direct functional inhibition of AKT1, EGFR, or STAT3. Moreover, Although HUH7 cells provide consistent results for early mechanistic research, their cancerous characteristics make it

difficult to apply findings to primary human hepatocytes. It's crucial to validate these results in non-tumorigenic models such as HepaRG, primary hepatocytes, and co-cultures to ensure their relevance for translation.

Challenges arise from the pharmacokinetics of andrographolide, as its poor solubility, Pgp efflux, and rapid metabolism result in low systemic exposure. Addressing these challenges (for instance, through advanced formulations or prodrugs) is crucial to unlock its therapeutic potential in MAFLD.

Conclusion

This comprehensive study, utilizing a multi-faceted methodology that includes computational network pharmacology, molecular docking, and experimental validation, offers substantial and converging evidence regarding the therapeutic efficacy of andrographolide in the context of MAFLD. Our in silico investigations laid a solid molecular groundwork, forecasting a favorable safety profile characterized by a low risk of hepatotoxicity, while also pinpointing a network of essential targets within critical MAFLD pathways that encompass inflammation, metabolism, and cellular signaling. Importantly, these computational forecasts were corroborated through experimental means. In vitro studies revealed that andrographolide significantly reduced OA-induced lipid accumulation in HUH7 hepatocytes, thereby affirming its direct anti-steatotic properties. Furthermore, the results from qPCR indicated that andrographolide specifically lowered the mRNA expression of AKT1, EGFR, and STAT3 mRNA in steatotic cells. This suggests that it may influence processes like lipogenesis, cell proliferation, and inflammation. However, it's important to note that these effects might be a result of decreased steatosis. To establish direct mechanistic effects, further validation at the protein level and functional assays are necessary. Crucially, AKT1 and STAT3 activities are primarily regulated through phosphorylation, which cannot be assessed by qPCR. Protein-level validation (Western blot for p-AKT1 Ser473, p-STAT3 Tyr705, and total EGFR) is absent in this study and is required to establish functional target engagement. The alignment of robust predicted binding affinities derived from docking studies with the noted downregulation of these target genes provides a coherent hypothesis for a multi-target mechanism of action. However, this hypothesis requires experimental confirmation at the protein level. Andrographolide seems to concurrently influence interrelated pathological processes in MAFLD steatosis, inflammation, and insulin resistance via a polypharmacological effect. Although the encouraging anti-steatotic and anti-inflammatory characteristics position andrographolide as a strong candidate for MAFLD treatment, subsequent research must tackle its pharmacokinetic and pharmacodynamic safety liabilities. Future efforts should concentrate on enhancing bioavailability, verifying in vivo target engagement, and assessing its effectiveness in advanced experimental models of steatohepatitis and fibrosis to fully unlock its translational potential.

Ethical Consent

This study was conducted in accordance with the ethical principles outlined in the Declaration of Helsinki. The research protocol was reviewed and approved by the Institutional Ethics Committee of Abadan University of Medical Sciences (Ethical Code: IR.ABADANUMS.REC.1405.004).

Acknowledgments

The authors used the web-based AI writing tools Ahrefs Paragraph Rewriter (Ahrefs Pte. Ltd., web version, https://ahrefs.com/writing-tools/paragraph-rewriter) and EnglishEdit AI (web version, https://englishedit.ai/) solely for copy-editing, including grammar correction, language refinement, readability enhancement, and improvement of manuscript structure. The authors reviewed the terms of use of these AI tools and confirm that their use complies with the journal's publication requirements and is suitable for publication. Following AI-assisted editing, the authors carefully reviewed and revised the entire manuscript, verified the originality and accuracy of all scientific content and references, and take full responsibility for the integrity and final content of the manuscript.

Author Contributions

All authors made a significant contribution to the work reported, whether that is in the conception, study design, execution, acquisition of data, analysis and interpretation, or in all these areas; took part in drafting, revising or critically reviewing the article; gave final approval of the version to be published; have agreed on the journal to which the article has been submitted; and agree to be accountable for all aspects of the work.

Funding

This study was supported by Abadan University of Medical Sciences under Grant No. 2361 and approved by the Institutional Ethics Committee (Ethical Code: IR.ABADANUMS.REC.1405.004).

Disclosure

The author declare no competing interests in this work.

References

1. Abdelhameed F, Kite C, Lagojda L, et al. Non-invasive Scores and Serum Biomarkers for Fatty Liver in the Era of Metabolic Dysfunction-associated Steatotic Liver Disease (MASLD): a Comprehensive Review From NAFLD to MAFLD and MASLD. *Curr Obes Rep*. 2024;13(3):510–531. doi:10.1007/s13679-024-00574-z
2. Pipitone RM, Ciccioli C, Infantino G, et al. MAFLD: a multisystem disease. *Ther Adv Endocrinol Metab*. 2023;14:20420188221145549. doi:10.1177/20420188221145549
3. Mahmoudi A, Jamialahmadi T, Johnston TP, Sahebkar A. Impact of fenofibrate on NAFLD/NASH: a genetic perspective. *Drug Discovery Today*. 2022;27(8):2363–2372. doi:10.1016/j.drudis.2022.05.007
4. Mahmoudi A, Moallem SA, Johnston TP, Sahebkar A. Liver Protective Effect of Fenofibrate in NASH/NAFLD Animal Models. *PPAR Res*. 2022;2022(1):5805398. doi:10.1155/2022/5805398
5. Mahmoudi A, Butler AE, Jamialahmadi T, Sahebkar A. The role of exosomal miRNA in nonalcoholic fatty liver disease. *J Cell Physiol*. 2022;237(4):2078–2094. doi:10.1002/jcp.30699
6. Mahmoudi A, Rostami M, Mahdi Hajihasani M, Sukhorukov VN, Kesharwani P, Sahebkar A. siRNA-mediated gene silencing for non-alcoholic fatty liver disease: a comprehensive review of molecular targets. *Eur Polym J*. 2024;208:112866. doi:10.1016/j.eurpolymj.2024.112866
7. Godinez-Leiva E, Bril F. Nonalcoholic Fatty Liver Disease (NAFLD) for Primary Care Providers: beyond the Liver. *Curr Hypertens Rev*. 2021;17(2):94–111. doi:10.2174/1573402116999201209203534
8. Liu AN, Xu CF, Liu YR, et al. Secondary bile acids improve risk prediction for non-invasive identification of mild liver fibrosis in nonalcoholic fatty liver disease. *Aliment Pharmacol Ther*. 2023;57(8):872–885. doi:10.1111/apt.17362
9. Xu Y, An Z, Wang S, et al. Dual role of pregnane X receptor in nonalcoholic fatty liver disease. *Curr Mol Pharmacol*. 2024;17:e18761429259143.
10. Vikal A, Maurya R, Patel P, Kurmi BD. Andrographis paniculata in fatty liver disease: mechanisms, nanocarrier approaches, and therapeutic potential. *Phytomedicine Plus*. 2025;5(4):100903. doi:10.1016/j.phyplu.2025.100903
11. Burgos RA, Alarcón P, Quiroga J, Manosalva C, Hancke J. Andrographolide, an anti-inflammatory multitarget drug: all roads lead to cellular metabolism. *Molecules*. 2020;26(1):5. doi:10.3390/molecules26010005
12. Qu J, Liu Q, You G, et al. Advances in ameliorating inflammatory diseases and cancers by andrographolide: pharmacokinetics, pharmacodynamics, and perspective. *Med Res Rev*. 2022;42(3):1147–1178. doi:10.1002/med.21873
13. Zeng B, Wei A, Zhou Q, et al. Andrographolide: a review of its pharmacology, pharmacokinetics, toxicity and clinical trials and pharmaceutical researches. *Phytother Res*. 2022;36(1):336–364. doi:10.1002/ptr.7324
14. Qin X, Wang X, Tian M, et al. The role of Andrographolide in the prevention and treatment of liver diseases. *Phytomedicine*. 2023;109:154537. doi:10.1016/j.phymed.2022.154537
15. Li Y, He S, Tang J, et al. Andrographolide inhibits inflammatory cytokines secretion in LPS-stimulated RAW264.7 cells through suppression of NF-κB/MAPK signaling pathway. *Evid Based Complement Alternat Med*. 2017;2017(1):8248142. doi:10.1155/2017/8248142
16. Ding Y, Shi C, Chen L, et al. Effects of andrographolide on postoperative cognitive dysfunction and the association with NF-κB/MAPK pathway. *Oncol Lett*. 2017;14(6):7367–7373. doi:10.3892/ol.2017.7088
17. Yan H, Huang Z, Bai Q, et al. Natural product andrographolide alleviated APAP-induced liver fibrosis by activating Nrf2 antioxidant pathway. *Toxicology*. 2018;396–397:1–12. doi:10.1016/j.tox.2018.01.007
18. Shan X, Li S, Liu J, et al. The therapeutic potential of andrographolide and its derivatives in inflammatory diseases. *Pharmacol Res Perspect*. 2025;13(5):e70161. doi:10.1002/prp2.70161
19. Ran LS, Wu YZ, Gan YW, et al. Andrographolide ameliorates hepatic steatosis by suppressing FATP2-mediated fatty acid uptake in mice with nonalcoholic fatty liver disease. *J Nat Med*. 2023;77(1):73–86. doi:10.1007/s11418-022-01647-w
20. Chen CC, Chuang WT, Lin AH, et al. Andrographolide inhibits adipogenesis of 3T3-L1 cells by suppressing C/EBPβ expression and activation. *Toxicol Appl Pharmacol*. 2016;307:115–122. doi:10.1016/j.taap.2016.07.021
21. Kaewkittikhun M, Boonmuen N, Kheolamai P, et al. Andrographolide reduces lipid droplet accumulation in adipocytes derived from human bone marrow mesenchymal stem cells by suppressing regulators of adipogenesis. *J Agric Food Chem*. 2021;69(32):9259–9269. doi:10.1021/acs.jafc.1c02724
22. Liu YT, Chen HW, Lii CK, et al. A diterpenoid, 14-deoxy-11, 12-didehydroandrographolide, in andrographis paniculata reduces steatohepatitis and liver injury in mice fed a high-fat and high-cholesterol diet. *Nutrients*. 2020;12(2):1.
23. Cabrera D, Wree A, Povero D, et al. Andrographolide ameliorates inflammation and fibrogenesis and attenuates inflammasome activation in experimental non-alcoholic steatohepatitis. *Sci Rep*. 2017;7(1):3491. doi:10.1038/s41598-017-03675-z
24. Xu G, Ma T, Zhou C, Zhao F, Peng K, Li B. Combination of pirfenidone and andrographolide ameliorates hepatic stellate cell activation and liver fibrosis by mediating TGF-β/Smad signaling pathway. *Anal Cell Pathol (Amst)*. 2024;2024(1):2751280. doi:10.1155/2024/2751280
25. Abdulaziz Bardi D, Halabi MF, Hassandarvish P, et al. Andrographis paniculata leaf extract prevents thioacetamide-induced liver cirrhosis in rats. *PLoS One*. 2014;9(10):e109424. doi:10.1371/journal.pone.0109424
26. Das S, Pradhan GK, Das S, Nath D, Das SK. Enhanced protective activity of nano formulated andrographolide against arsenic induced liver damage. *Chem Biol Interact*. 2015;242:281–289. doi:10.1016/j.cbi.2015.10.011
27. Song Y, Wu X, Yang D, et al. Protective effect of andrographolide on alleviating chronic alcoholic liver disease in mice by inhibiting nuclear factor kappa B and tumor necrosis factor alpha activation. *J Med Food*. 2020;23(4):409–415. doi:10.1089/jmf.2019.4471

28. Peng Y, Demidchik V, Li Y, et al. Characterization of andrographolide-loaded exosome-like nanoparticles from Nauclea officinalis and their modulation of inflammatory and lipid metabolic pathologies in WRL68 cells. *Fitoterapia*. 2026;190:107179. doi:10.1016/j.fitote.2026.107179
29. Wang J, Tao H, Wang Z, et al. Application of network pharmacology, molecular docking, and in vitro experimental evaluation to decipher the anti-inflammatory mechanisms of cirsium japonicum. *Appl Sci*. 2024;14(21):9687. doi:10.3390/app14219687
30. Mahmoudi A, Butler AE, Majeed M, Banach M, Sahebkar A. Investigation of the Effect of Curcumin on Protein Targets in NAFLD Using Bioinformatic Analysis. *Nutrients*. 2022;14(7):1331. doi:10.3390/nu14071331
31. Mahmoudi A, Jalili A, Butler AE, Aghaee-Bakhtiari SH, Jamialahmadi T, Sahebkar A. Exploration of the Key Genes Involved in Non-alcoholic Fatty Liver Disease and Possible MicroRNA Therapeutic Targets. *J Clin Exper Hepatol*. 2024;14(4):101365. doi:10.1016/j.jceh.2024.101365
32. Mahmoudi A, Hajihasani MM, Majeed M, Jamialahmadi T, Sahebkar A. Effect of Calebin-A on Critical Genes Related to NAFLD: a Protein-Protein Interaction Network and Molecular Docking Study. *Current Genomics*. 2024;25(2):120–139. doi:10.2174/0113892029280454240214072212
33. Dixit N, Motwani H, Patel SK, Rawal RM, Solanki HA. Decoding the mechanism of andrographolide to combat hepatocellular carcinoma: a network pharmacology integrated molecular docking and dynamics approach. *J Biomol Struct Dyn*. 2024;42(19):10237–10255. doi:10.1080/07391102.2023.2256866
34. Zhang Y, Liu S, Liang X, Yin L, He C. Integrating Network Pharmacology, Molecular Docking, and Experimental Validation: andrographolide Attenuates Acute Liver Injury via the NLRP3/Caspase-1/GSDMD-Mediated Pyroptosis Pathway. *Biomolecules*. 2025;15(12):1743. doi:10.3390/biom15121743
35. Yin Y, He J, Fang Y, Wei M, Zhang W. Andrographolide as a Multi-Target Therapeutic Agent in Diabetic Nephropathy: insights into STAT3/PI3K/Akt Pathway Modulation. *Biomol Ther (Seoul)*. 2025;33(3):529–543. doi:10.4062/biomolther.2024.209
36. Zhang Q, Zhang Y, Wang C, et al. Andrographolide attenuates pulmonary fibrosis by covalently targeting Ptges3 and disrupting the Ptges3-Hsp90-NF-κB axis. *J Adv Res*. 2026;2026:1.
37. He X, Ma J, Yan X, et al. CDT1 is a Potential Therapeutic Target for the Progression of NAFLD to HCC and the Exacerbation of Cancer. *Curr Genomics*. 2025;26(3):225–243. doi:10.2174/0113892029313473240919105819
38. Sotoudeheian M. Galectin-3 and Severity of Liver Fibrosis in Metabolic Dysfunction-Associated Fatty Liver Disease. *Protein Pept Lett*. 2024;31(4):290–304. doi:10.2174/0109298665301698240404061300
39. Banerjee P, Kemmler E, Dunkel M, Preissner R. ProTox 3.0: a webserver for the prediction of toxicity of chemicals. *Nucleic Acids Res*. 2024;52(W1):W513–W20. doi:10.1093/nar/gkae303
40. Xie Y, Hu W, Chen X, et al. Identification and validation of autophagy-related genes in exogenous sepsis-induced acute respiratory distress syndrome. *Immun Inflamm Dis*. 2022;10(10):e691. doi:10.1002/iid3.691
41. Pasamba EC, Orda MA, Villanueva BHA, Tsai P-W, Tayo LL. Transcriptomic Analysis of Hub Genes Reveals Associated Inflammatory Pathways in Estrogen-Dependent Gynecological Diseases. *Biology*. 2024;13(6):397. doi:10.3390/biology13060397
42. Hetényi C, van der Spoel D. Efficient docking of peptides to proteins without prior knowledge of the binding site. *Protein Sci*. 2002;11(7):1729–1737. doi:10.1110/ps.0202302
43. Trott O, Olson AJ. AutoDock Vina: improving the speed and accuracy of docking with a new scoring function, efficient optimization, and multithreading. *J Comput Chem*. 2010;31(2):455–461. doi:10.1002/jcc.21334
44. Mahmoudi A, Jalili A, Aghaee-Bakhtiari SH, et al. Analysis of the therapeutic potential of miR-124 and miR-16 in non-alcoholic fatty liver disease. *J diabet complicat*. 2024;38(4):108722. doi:10.1016/j.jdiacomp.2024.108722
45. Ye L, Wang T, Tang L, et al. Poor oral bioavailability of a promising anticancer agent andrographolide is due to extensive metabolism and efflux by P-glycoprotein. *J Pharm Sci*. 2011;100(11):5007–5017. doi:10.1002/jps.22693
46. Songvut P, Boonyarattanasoonthorn T, Nuengchamnong N, et al. Enhancing oral bioavailability of andrographolide using solubilizing agents and bioenhancer: comparative pharmacokinetics of Andrographis paniculata formulations in beagle dogs. *Pharm Biol*. 2024;62(1):183–194. doi:10.1080/13880209.2024.2311201
47. Patil R, Jain V. Andrographolide: a Review of Analytical Methods. *J Chromatogr Sci*. 2021;59(2):191–203. doi:10.1093/chromsci/bmaa091
48. Panossian A, Hovhannisyan A, Mamikonyan G, et al. Pharmacokinetic and oral bioavailability of andrographolide from Andrographis paniculata fixed combination Kan Jang in rats and human. *Phytomedicine*. 2000;7(5):351–364. doi:10.1016/S0944-7113(00)80054-9
49. Chandrasekaran CV, Thiyagarajan P, Sundarajan K, et al. Evaluation of the genotoxic potential and acute oral toxicity of standardized extract of Andrographis paniculata (KalmCold). *Food Chem Toxicol*. 2009;47(8):1892–1902. doi:10.1016/j.fct.2009.05.006
50. Sharifuddin Y, Parry EM, Parry JM. The genotoxicity and cytotoxicity assessments of andrographolide in vitro. *Food Chem Toxicol*. 2012;50(5):1393–1398. doi:10.1016/j.fct.2012.01.039
51. Li X, Yuan W, Wu J, Zhen J, Sun Q, Yu M. Andrographolide, a natural anti-inflammatory agent: an update. *Front Pharmacol*. 2022;13:920435. doi:10.3389/fphar.2022.920435
52. Hu W, Chen Y, Tan W, Wang Y, Huang D, Yuan H. Andrographolide inhibits the NF-κB signaling pathway and alleviates high-fat diet-induced hepatic inflammation in a mouse model of nonalcoholic fatty liver disease. *Nat Prod Commun*. 2025;20(2):1934578X241302020. doi:10.1177/1934578X241302020
53. Toppo E, Darvin SS, Esakkimuthu S, et al. Effect of two andrographolide derivatives on cellular and rodent models of non-alcoholic fatty liver disease. *Biomed Pharmacother*. 2017;95:402–411. doi:10.1016/j.biopha.2017.08.071
54. Lin L, Li R, Cai M, et al. Andrographolide Ameliorates Liver Fibrosis in Mice: involvement of TLR4/NF-κB and TGFβ1/Smad2 Signaling Pathways. *Oxid Med Cell Longev*. 2018;2018(1):7808656. doi:10.1155/2018/7808656
55. Li Q, Hou L, Su L, Wang X, Zhu Y, Fang B. Andrographolide Alleviates Liver Damage Caused by Salmonella in Mice by Inhibiting the PANoptosis Pathway. *Microorganisms*. 2026;14(4):936. doi:10.3390/microorganisms14040936
56. Tilg H, Moschen AR, Szabo G. Interleukin-1 and inflammasomes in alcoholic liver disease/acute alcoholic hepatitis and nonalcoholic fatty liver disease/nonalcoholic steatohepatitis. *Hepatology*. 2016;64(3):955–965. doi:10.1002/hep.28456
57. Xiao J, Tipoe GL. Inflammasomes in non-alcoholic fatty liver disease. *Front Biosci (Landmark Ed)*. 2016;21(4):683–695. doi:10.2741/4414
58. Mehal WZ. The inflammasome in liver injury and non-alcoholic fatty liver disease. *Dig Dis*. 2014;32(5):507–515. doi:10.1159/000360495
59. Ravindran R, Loebbermann J, Nakaya HI, et al. The amino acid sensor GCN2 controls gut inflammation by inhibiting inflammasome activation. *Nature*. 2016;531(7595):523–527. doi:10.1038/nature17186

60. Zhou J, Ong CN, Hur GM, Shen HM. Inhibition of the JAK-STAT3 pathway by andrographolide enhances chemosensitivity of cancer cells to doxorubicin. *Biochem Pharmacol*. 2010;79(9):1242–1250. doi:10.1016/j.bcp.2009.12.014
61. Li L, S-h L, J-p J, Liu C, L-l J. Investigating pharmacological mechanisms of andrographolide on non-alcoholic steatohepatitis (NASH): a bioinformatics approach of network pharmacology. *Chinese Herbal Medicines*. 2021;13(3):342–350. doi:10.1016/j.chmed.2021.05.001
62. Wang S, Li H, Chen S, et al. Andrographolide induces apoptosis in human osteosarcoma cells via the ROS/JNK pathway. *Int J Oncol*. 2020;56 (6):1417–1428. doi:10.3892/ijo.2020.5032
63. Xia Y-F, Ye B-Q, Li Y-D, et al. Andrographolide attenuates inflammation by inhibition of NF-κB activation through covalent modification of reduced cysteine 62 of p50. *J Immunol*. 2004;173(6):4207–4217. doi:10.4049/jimmunol.173.6.4207
64. Luedde T, Schwabe RF. NF-κB in the liver—linking injury, fibrosis and hepatocellular carcinoma. *Nat Rev Gastroenterol Hepatol*. 2011;8 (2):108–118. doi:10.1038/nrgastro.2010.213
65. Luedde T, Beraza N, Trautwein C. Evaluation of the role of nuclear factor-kappaB signaling in liver injury using genetic animal models. *J Gastroenterol Hepatol*. 2006;21(Suppl 3):S43–6.
66. Cai Q, Zhang W, Sun Y, et al. Study on the mechanism of andrographolide activation. *Front Neurosci*. 2022;16:977376. doi:10.3389/ fnins.2022.977376
67. Wang S, Tao J, Chen H, et al. Ablation of Akt2 and AMPKα2 rescues high fat diet-induced obesity and hepatic steatosis through Parkin-mediated mitophagy. *Acta Pharm Sin B*. 2021;11(11):3508–3526. doi:10.1016/j.apsb.2021.07.006
68. Kaewpiboon C, Boonnak N, Salae AW, Pakdeepromma S, Yawut N, Chung YH. Andrographolide targets EGFR to impede epithelial-mesenchymal transition in human breast cancer cells. *J Pharm Biomed Anal*. 2024;248:116267. doi:10.1016/j.jpba.2024.116267
69. Zhai T, Cai L, Jia X, et al. IGFBP2 functions as an endogenous protector against hepatic steatosis via suppression of the EGFR-STAT3 pathway. *Mol Metab*. 2024;89:102026. doi:10.1016/j.molmet.2024.102026
70. Nie X, Chen SR, Wang K, et al. Attenuation of innate immunity by andrographolide derivatives through NF-κB Signaling pathway. *Sci Rep*. 2017;7 (1):4738. doi:10.1038/s41598-017-04673-x
71. Peng S, Hang N, Liu W, et al. Andrographolide sulfonate ameliorates lipopolysaccharide-induced acute lung injury in mice by down-regulating MAPK and NF-κB pathways. *Acta Pharm Sin B*. 2016;6(3):205–211. doi:10.1016/j.apsb.2016.02.002
72. Gao J, Peng S, Shan X, et al. Inhibition of AIM2 inflammasome-mediated pyroptosis by Andrographolide contributes to amelioration of radiation-induced lung inflammation and fibrosis. *Cell Death Dis*. 2019;10(12):957. doi:10.1038/s41419-019-2195-8
73. Sato H, Hiraki M, Namba T, et al. Andrographolide induces degradation of mutant p53 via activation of Hsp70. *Int J Oncol*. 2018;53(2):761–770. doi:10.3892/ijo.2018.4416
74. Liao W, Lim AYH, Tan WSD, Abisheganaden J, Wong WSF. Restoration of HDAC2 and Nrf2 by andrographolide overcomes corticosteroid resistance in chronic obstructive pulmonary disease. *Br J Pharmacol*. 2020;177(16):3662–3673. doi:10.1111/bph.15080
75. Qi X, Zheng S, Ma M, et al. Curcumol suppresses CCF-mediated hepatocyte senescence through blocking LC3B-Lamin B1 interaction in alcoholic fatty liver disease. *Front Pharmacol*. 2022;13:912825. doi:10.3389/fphar.2022.912825
76. Li A, Nie T, Wang X, Ma J. Hesperidin ameliorates hepatocyte cell cycle disruption, apoptosis, and necroptosis in mice with nonalcoholic fatty liver disease via the VEGFA-PI3K/AKT pathway. *Int Immunopharmacol*. 2025;163:115304. doi:10.1016/j.intimp.2025.115304